ARMY RESEARCH LABORATORY

Corrosion Screening of EV31A Magnesium and Other Magnesium Alloys Using Laboratory-Based Accelerated Corrosion and Electro-chemical Methods

by Brian E. Placzankis, Joseph P. Labukas, Elizabeth Charleton, and Chris E. Miller

ARL-TR-6899 **July 2014**

NOTICES

Disclaimers

The findings in this report are not to be construed as an official Department of the Army position unless so designated by other authorized documents.

Citation of manufacturer's or trade names does not constitute an official endorsement or approval of the use thereof.

Destroy this report when it is no longer needed. Do not return it to the originator.

Army Research Laboratory
Aberdeen Proving Ground, MD 21005-5066

ARL-TR-6899 **July 2014**

Corrosion Screening of EV31A Magnesium and Other Magnesium Alloys Using Laboratory-Based Accelerated Corrosion and Electro-chemical Methods

Brian E. Placzankis, Joseph P. Labukas, Elizabeth Charleton, and Chris E. Miller
Weapons and Materials Research Directorate, ARL

REPORT DOCUMENTATION PAGE	Form Approved OMB No. 0704-0188

1. REPORT DATE *(DD-MM-YYYY)*	2. REPORT TYPE	3. DATES COVERED (08/01/2013 – To-02/01/2014)
July 2014	Final	August 2013–February 2014

4. TITLE AND SUBTITLE
Corrosion Screening of EV31A Magnesium and Other Magnesium Alloys Using Laboratory-Based Accelerated Corrosion and Electro-chemical Methods

5a. CONTRACT NUMBER

5b. GRANT NUMBER

5c. PROGRAM ELEMENT NUMBER

6. AUTHOR(S)
Brian E. Placzankis, Joseph P. Labukas, Elizabeth Charleton, and Chris E. Miller

5d. PROJECT NUMBER

5e. TASK NUMBER

5f. WORK UNIT NUMBER

7. PERFORMING ORGANIZATION NAME(S) AND ADDRESS(ES)
U.S. Army Research Laboratory
ATTN: RDRL-WMM-C
Aberdeen Proving Ground, MD 21005-5066

8. PERFORMING ORGANIZATION REPORT NUMBER
ARL-TR-6899

9. SPONSORING/MONITORING AGENCY NAME(S) AND ADDRESS(ES)

10. SPONSOR/MONITOR'S ACRONYM(S)

11. SPONSOR/MONITOR'S REPORT NUMBER(S)

12. DISTRIBUTION/AVAILABILITY STATEMENT
Approved for public release; distribution is unlimited.

13. SUPPLEMENTARY NOTES

14. ABSTRACT
Test specimens of EV31A and other prospective magnesium alloys for U.S. Department of Defense systems were identically prepared and exposed under bare, uncoated conditions in chamber-based laboratory-accelerated corrosion test methods to assess their relative susceptibilities to general and pitting corrosion attack. The methods used were ASTM B117 neutral salt fog (NSF) and General Motors (GM) Standard 9540P cyclic accelerated corrosion. The NSF specimens were compared at intervals of 18, 72, and 168 h. The GM 9540P specimens were assessed at 1-, 5-, and 10-cycle intervals. The visual corrosion assessments were graphically obtained using flatbed scanning techniques. Following the exposures, mass loss measurements were obtained for all specimens to determine corrosion rates. Electro-chemical evaluations of corrosion susceptibility for each of the alloys were performed using potentiodynamic polarization. Based on the results of these studies, the overall corrosion resistance for EV31A was found to be good, and its relative susceptibility to general corrosion attack compared with the current military specification alloy AZ31B is discussed.

15. SUBJECT TERMS
corrosion, magnesium, alloys, EV31A, E21, ZE41A, AZ31B, AZ91C, WE43B, AMX602, ZAXE1711, salt fog, cyclic corrosion, GM 9540P

16. SECURITY CLASSIFICATION OF:			17. LIMITATION OF ABSTRACT	18. NUMBER OF PAGES	19a. NAME OF RESPONSIBLE PERSON
a. REPORT	b. ABSTRACT	c. THIS PAGE			Brian E. Placzankis
Unclassified	Unclassified	Unclassified	UU	40	19b. TELEPHONE NUMBER (*Include area code*) 410-306-2989

Standard Form 298 (Rev. 8/98)
Prescribed by ANSI Std. Z39.18

Contents

List of Figures

List of Tables

Acknowledgments

The authors thank Tyrone Jones of the U.S. Army Research Laboratory Armor Mechanisms Branch, Steve Brown of the U.S. Naval Air Systems Command, and Katsuyoshi Kondoh of the Joining and Welding Research Institute of Osaka University, Japan, for supplying magnesium samples used to produce the specimens in this study. The authors also thank Magnesium Elektron (Madison, IL) for supplying additional magnesium alloy samples and detailed properties for some of the alloys studied.

1. Introduction

The U.S. Department of Defense (DOD) has historically used magnesium (Mg) in various applications, the majority being military aircraft, but despite its weight advantage over other materials, Mg has been limited in wider use (*1*). The prevailing factors limiting greater usage remain centered on poor corrosion resistance and persistent concerns about flame resistance. Recent regulatory pressures such as updated Corporate Average Fuel Economy standards have renewed interest in lighter-weight designs to comply with the mandates for more fuel-efficient automotive systems (*2*). The push for lighter-weight designs to increase fuel economy for civilian vehicles coincides with the renewed interest in Mg for ground-based defense applications such as structures and armor (*3*–*5*).

In 2009, the first U.S. military specification (MILSPEC) for Mg armor plate was established. This specification, known as MIL-DTL-32333 (*6*), Armor Plate, Magnesium Alloy, AZ31B, Applique, sets minimum acceptance values for mechanical properties, ballistics, and corrosion resistance in the bare, uncoated state. These minimum values are critical for manufacturers to deliver consistent and predictable materials performance for vehicles and weapons platforms. The addition of a minimum acceptance value for corrosion resistance was a critical parameter for the specification creation and is unique to Mg armor plates. Although significant research and development efforts (*7*) to expand the available Mg alloy plate have occurred since establishing MIL-DTL-32333, as of 2013 AZ31B-H24 remains the sole qualified alloy for this specification.

This report provides additional basic corrosion screening data using the two most common laboratory-accelerated corrosion methods and electro-chemical polarization. Although these methods are useful for understanding alloy corrosion, predicting the long-term corrosion performance is complicated and requires more rigorous testing in a variety of environments. As with aluminum (Al) and steel materials, additional corrosion vulnerability data from other sources such as the Aberdeen Test Center Automotive Test Track, longer-term outdoor exposures, and prior corrosion data from actual fielded platforms should play greater roles in the final design decision process. This study consolidates and extends previous work, provides new data on the Magnesium Elektron alloy EV31A (*8*) (also known by the trade name Elektron 21), and adds baseline electro-chemical data for previously screened alloys (*9*).

2. Experimental Procedure

In order to assess the inherent corrosion resistance capabilities of bare, unprotected Mg alloys currently in use or proposed for use by the U.S. DOD, a wide selection of cast and wrought Mg alloys were chosen from aviation, industry, and specialty alloys proposed for ground

applications. The detailed list of Mg including pure melt-grade Mg followed by Mg alloys of various tempers, in alphanumerical order, included commercially pure (CP) melt-grade Mg (CPMg 9980B) (*10*), AMX602 (*11*), AZ31B-H24 (*12*), AZ91C-T6 (*13*), EV31A-T6, WE43B-T5 (*13*), ZAXE1711 (*14*), and ZE41A (*13*). The chemical composition and mechanical properties of these alloys are listed in tables 1 and 2, respectively.

Table 1. Chemical compositions for Mg alloys (%).

Element (%)/Alloy	CPMg 9980B	AMX602	AZ31B	AZ91C	EV31A	WE43B	ZAXE1711	ZE41A
Aluminum	-	6.0	2.5 - 3.5	8.1 - 9.3	-	-	7.0	-
Manganese	0.10 max	0.5	0.2 - 1.0	0.13 - 0.35	-	0.03 max	-	0.15 max
Zinc	-	-	0.6 - 1.4	0.40 - 1.0	0.20 - 0.50	-	1.0	3.5 - 5.0
Yttrium	-	-	-	-	-	3.7 - 4.3	-	
Neodymium	-	-	-	-	2.6 - 3.1	2.0 - 2.5	-	
Gadolinium					1.0 - 1.7		-	
Rare Earths (total)	-	-	-	-	-	2.4 - 4.4	-	0.75 - 1.75
Zirconium	-	-	-	-	0.4 - 1.0	0.40 - 1.0	-	0.40 - 1.0
Silicon	-	-	0.10 max	0.30 max	-	-	-	-
Copper	0.02 max	-	0.05 max	0.10 max	0.01 max	0.02 max	-	0.10 max
Nickel	0.005 max	-	0.005 max	0.01 max	0.0020 max	0.005 max	-	0.01 max
Iron	-	-	0.005 max	-	0.010 max	0.010 max	-	-
Calcium	-	2	0.04 max	-	-	-	1.0	-
Lanthanum	-	-	-	-	-	-	1.0	-
Lithium	-	-	-	-	-	0.2 max	-	-
Lead	0.01 max	-	-	-	-	-	-	-
Silver					0.05 max		-	
Tin	0.01 max	-	-	-	-	-	-	-
Zinc + Silver	-	-	-	-	-	0.20 max	-	-
Others Each	0.05 max	-	-	-	0.01	0.01 max	-	-
Other Rare Earths					0.4 max		-	
Others Total	-	-	0.30 max	0.30 max	-	-	-	0.30 max
Magnesium	99.80 min	REM	REM	REM	REM	REM	REM	REM

Table 2. Mechanical properties for Mg alloys.

Property/Alloy	CPMg	AMX602	AZ31B-H24	AZ91C	EV31A	WE43B-T5	ZAXE1711	ZE41A
Yield Stress (MPa)	21	309	125	100	145	180	270	134
Ultimate Tensile Stress (MPa)	90	357	235	170	248	250	382	193
Elongation (%)	4	19.9	7	2	2	7	18.1	3
Form	Cast	Extruded	Rolled	Cast	Cast	Wrought	Extruded	Cast
Density (g/cm3)	1.74	1.78	1.77	1.83	1.82	1.84	1.78	1.84

For simplicity's sake, mechanical properties listed for the powder and extruded alloys AMX602 and ZAXE1711 were average values obtained using the longitudinal extruded direction from the three bars prepared from each alloy using temper temperatures listed in table 3.

Table 3. Temper temperatures used for AMX602 and ZAXE1711.

Designation and Tempering Temperature (º C)	
AMX602	ZAXE1711
1: 350	B: 350
2: 300	C: 250
3: 250	D: 200

The actual Mg specimens were cut to 1.75- × 1.5- × 0.25-in nominal dimensions using a water-cooled nonmetallic abrasive blade saw (Buehler, Lake Bluff, IL). When cutting the specimens, outer or parent material adjacent to exposed surfaces were used. The preference for using outer surfaces of specimens was two-fold. For the cast alloys or alloys originating from ingots, the use of outer material was to minimize the grain size. For the wrought Mg, the outer surfaces were selected for the most accurate representation of the alloy as it would actually be used, and thus specimens were down-sectioned to 0.25 in via the short transverse plane with only the outward facing exterior surfaces used. All specimens were then surface finished to 600 grit using metallographic grinding techniques. Following grinding, all specimens were cleaned and rinsed using acetone. Due to the varieties of plates and ingots, there were slight variations in thickness precision among the specimens. To normalize weight loss data collected among the specimens, the sample dimensions and initial mass were measured in addition to the initial masses. Finally, following the measurements for dimensions and mass, the specimens were organized in racks as shown in figure 1, and then placed into their respective chambers.

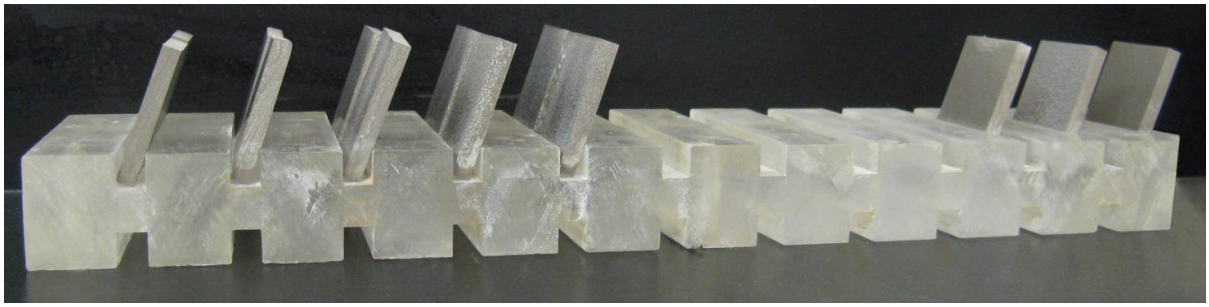

Figure 1. Corrosion rack configuration used for neutral salt fog (NSF) and General Motors (GM) Standard 9540P (*15*) exposures.

A standard wet-bottom style test Harshaw model 410 chamber was used for NSF testing and an Attotech model CCT-NC cyclic corrosion chamber was used for cyclic testing. The NSF operating parameters were in accordance with ASTM B117 (*16*) at 95 °F with saturated humidity and an atomized fog of 5% NaCl solution. In deference to previous studies where Mg alloys had corroded rapidly, the observation intervals for the specimens in NSF were modified to 4, 8, 18, 72, and 168 h rather than the 18, 72, and 168 h previously used for Al alloys. The image acquisition scans were made at the usual 18, 72, and 168 h with 4 and 8 h optional. If severe corrosion was observed early at 4 or 8 h, additional scans were then acquired. The GM 9540P (*15*) cyclic accelerated corrosion test consisted of 18 separate stages that included the following: saltwater spray using 0.9% NaCl, 0.1% $CaCl_2$, 0.25% $NaHCO_3$ test solution, high humidity, drying, ambient, and heated drying. The environmental conditions and duration of each stage for one complete cycle are provided in table 4.

Table 4. GM 9540P (*15*) cyclic corrosion test details.

Interval	Description	Time (min)	Temperature (±3C)
1	Ramp to Salt Mist	15	25
2	Salt Mist Cycle	1	25
3	Dry Cycle	15	30
4	Ramp to Salt Mist	70	25
5	Salt Mist Cycle	1	25
6	Dry Cycle	15	30
7	Ramp to Salt Mist	70	25
8	Salt Mist Cycle	1	25
9	Dry Cycle	15	30
10	Ramp to Salt Mist	70	25
11	Salt Mist Cycle	1	25
12	Dry Cycle	15	30
13	Ramp to Humidity	15	49
14	Humidity Cycle	480	49
15	Ramp to Dry	15	60
16	Dry Cycle	480	60
17	Ramp to Ambient	15	25
18	Ambient Cycle	480	25

In addition, the cyclic chamber was calibrated with standard cold-rolled steel mass loss calibration coupons as described in the GM 9540P test specification. Although the GM 9540P procedure was developed for steel substrates, previous studies (*17*) have shown that the cyclic nature of the exposure and the electrolyte used can also have a significant impact on the corrosion behavior of magnesium alloys. The observation and scanning intervals for the GM 9540P specimens were 1, 5, and 10 cycles.

To visually assess and characterize the corrosion, all specimens were scanned at 1200 dots per inch (dpi) optical resolution at their respective intervals using color flatbed scanning techniques. Specimens were vigorously rinsed under a stream of deionized water to remove loose corrosion products and thus better reveal the corrosion damage to the substrate surface. Following the rinse, the specimens were then allowed to dry prior to scanning. After the final optical scan at the conclusion of exposures in NSF and GM 9540P, and prior to final weighing to determine the mass loss, the specimens were all cleaned in accordance with ASTM G97 (*18*) to remove all remaining corrosion products. After the final weights were recorded, the corrosion rate in mils (thousands of an inch) per year (mpy) (*19*) was calculated using the following formula:

$$\text{mpy} = \frac{K \times (m_i - m_f}{(A \times T \times d)} \quad (1)$$

where K = constant (534,000 for mpy), m_i = initial mass (g), m_f = final mass (g), A = area (in^2), T = time (hours), and d = density (g/cm^2).

For GM 9540P cyclic corrosion where duration is measured in cycles, each cycle was normalized to 24 h. Therefore, the final exposure time in hours for the GM 9540P specimens was 240 h.

Potentiodynamic polarization of each Mg alloy was carried out in 3.5% (w/v) NaCl (aqueous) without stirring at ambient laboratory conditions. A Flat Cell (Princeton Applied Research, Oak Ridge, TN) was used and comprised approximately 250 mL of electrolyte, a Mg alloy working electrode, a Pt mesh counter electrode, and a saturated calomel electrode. The working electrode was polarized with a potentiostat (Ametek/Princeton Applied Research, VersaSTAT 3F) from 500 mV less than open circuit potential (OCP) to 500 mV greater than OCP at 1 mV/sec. The open circuit potential (OCP or E_{corr}) and corrosion current (I_{corr}) were calculated by fitting the linear portion of a plot of E versus I in the range of +/–100 mV around OCP using the RP fit function of the VersaStudio software (Ametek/Princeton Applied Research, version 2.40). For fitting the linear portion of the curve at such small overpotential, the constant β (Tafel slope) was fixed at 100 mV for both the anodic and cathodic branches. Reported values of I_{corr} and E_{corr} are the average of at least four potentiodynamic scans.

3. Results

Upon the start of chamber-accelerated corrosion testing, the decision was made to include additional scans of more actively corroding alloys. This decision was found to be fortuitous, as there was significant corrosion amongst some of the NSF specimens. These optional early image scan intervals at 4 and 8 h were needed for visually assessing the rapid corrosion progression for the more active alloys before the damage became too severe to observe the type and its origination.

3.1 Commercially Pure Magnesium (CP Mg)

The CP Mg examined was 9980B melt-grade Mg that is typically used for alloying additions to other base metals such as Al. As was obvious from scans in both NSF and from GM 9540P, the CP Mg sample was corroded more severely that any of the Mg alloys based on the high density of pits and visual mass loss, and the earlier 4- and 8-h observation intervals were indeed useful. The corrosion rate was so high that the NSF exposure was concluded at 72 h to avoid the risk of having no specimen remaining from which to measure mass loss at 168 h. The corrosion rates calculated from mass loss were two orders of magnitude higher than the worst of the remaining alloys for NSF and one order of magnitude greater for cyclic corrosion. Optical scans of the corrosion progression for CP Mg in NSF and GM 9540P are shown in figures 2 and 3, respectively.

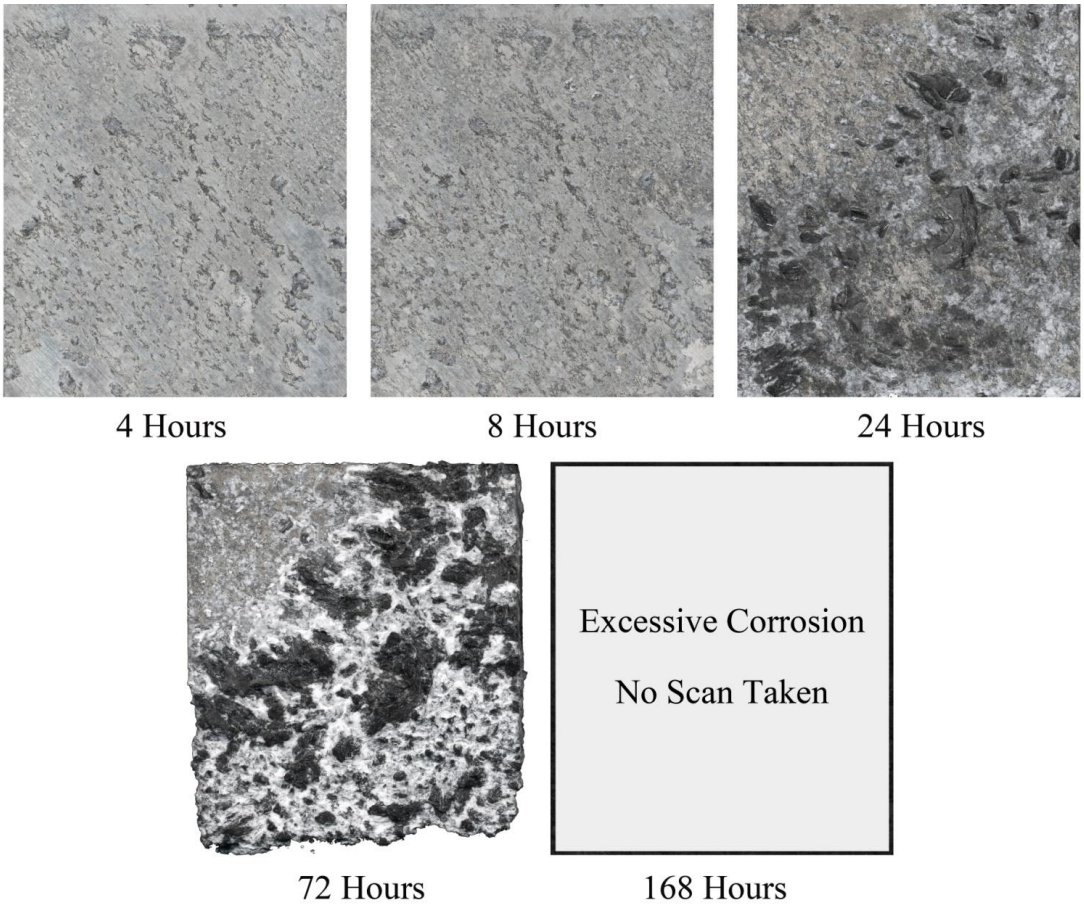

Figure 2. CP Mg after NSF.

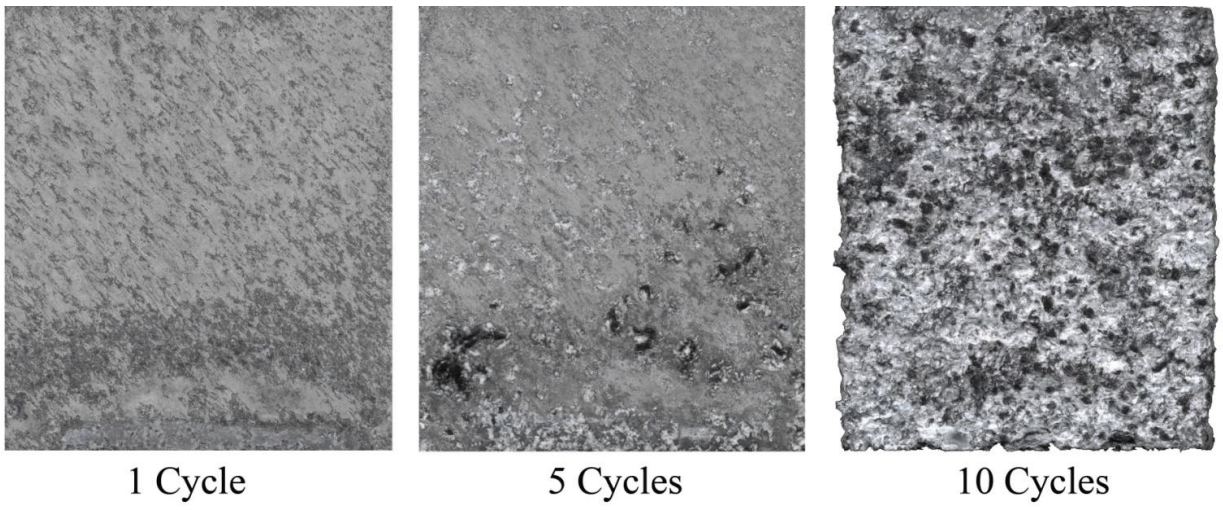

Figure 3. CP Mg after GM 9540P cyclic corrosion.

3.2 AMX602

This advanced powder-based alloy and ZAXE1711 (both from Japan) were produced using a Spinning Water Atomization Process (SWAP) to yield powder particles with very fine microstructures. These powders were compacted into a billet that was then hot-extruded into bars for further mechanical, ballistic, and corrosion studies (*16*). A schematic of the SWAP process and example of the powder produced is included in figure 4. This alloy contains amounts of Al similar to those found in AZ61 but lacks zinc and contains calcium. Images shown in figures 5 and 6 indicate very good response to accelerated corrosion environments with excellent performance under NSF and cyclic corrosion testing. AMX602 had the second lowest corrosion rate after AZ91C based on mass loss measurements.

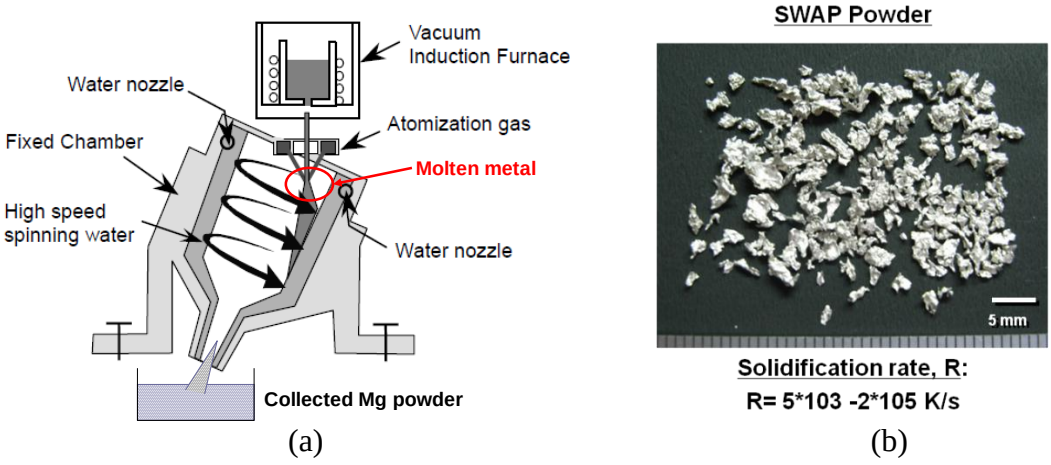

Figure 4. Schematic illustration of SWAP equipment (a) to produce rapidly solidified AMX602 and ZAXE1711 Mg alloy powders and (b) morphology of coarse Mg alloy powder prepared by SWAP (*16*).

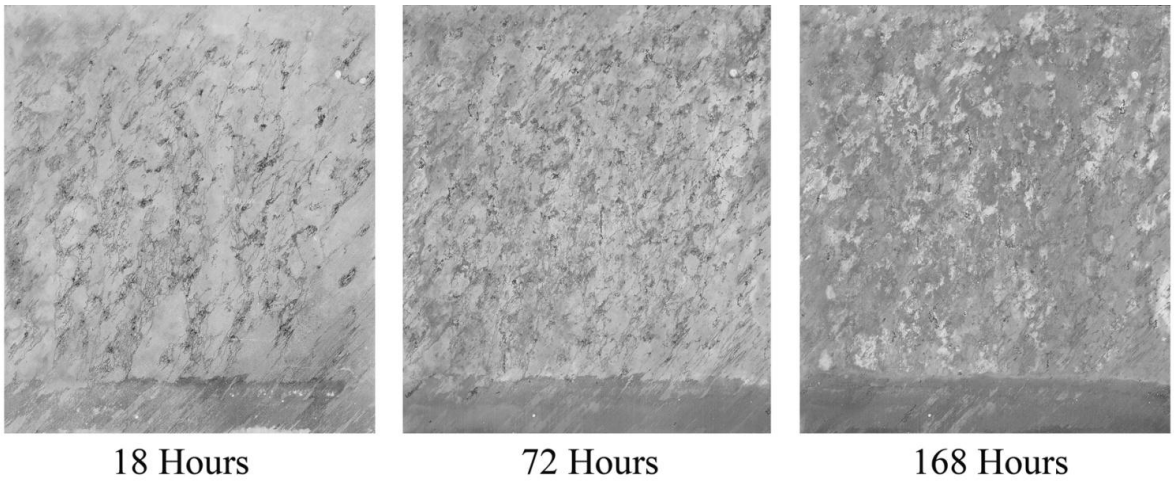

Figure 5. NSF corrosion of AMX602.

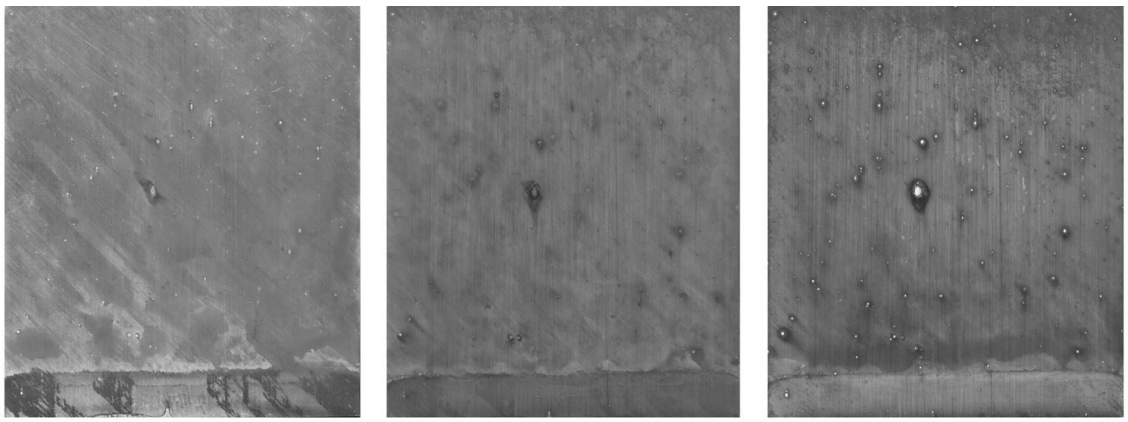

Figure 6. GM 9540P cyclic corrosion of AMX602.

3.3 AZ31B-H24

While CP Mg exists in this study as a scientific reference point, the AZ31B-H24 alloy can correspondingly be considered as the baseline engineering counterpart mainly due to its existence as the sole MILSPEC alloy for armor plates. The main alloying element in AZ31B-H24 is Al. This alloy is used for a variety of applications including aircraft fuselage materials and tooling plate. For armor, the AZ31B-H24 alloy was selected for its balanced mechanical properties and corrosion resistance. For both NSF and cyclic corrosion, the AZ31B-H24 performed as expected. The 7.1-mpy measurement for AZ31B-H24 in NSF was within the allowable acceptance range stated in the MILSPEC. The NSF corrosion initiated as filiform and was most visible at 72 h, and then propagated outward to encompass larger areas by the exposure conclusion at 168 h. The GM 9540P progression followed a similar mode but was less severe and stained darker. Figures 7–9 chronicle the corrosion of AZ31B-H24 including a close-up of the NSF filiform corrosion in figure 8.

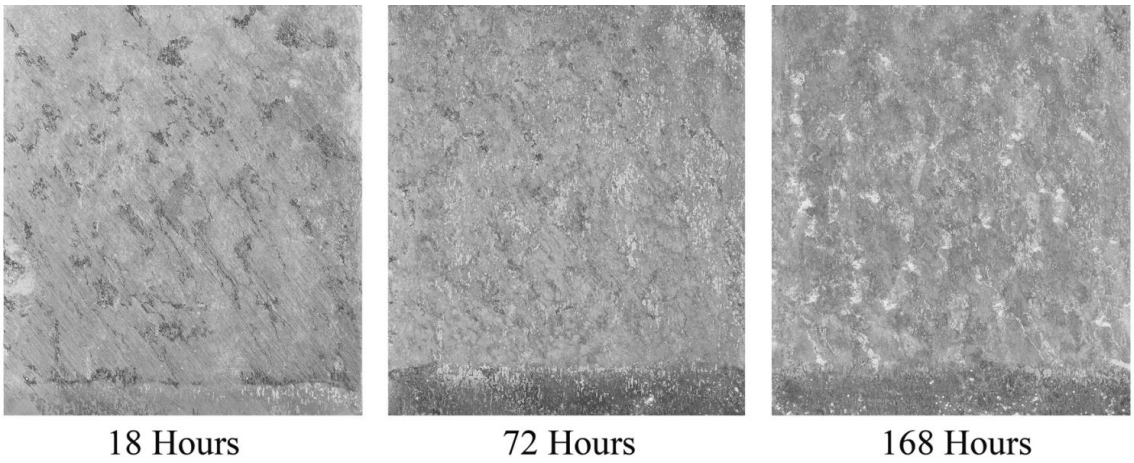

Figure 7. NSF corrosion of AZ31B-H24.

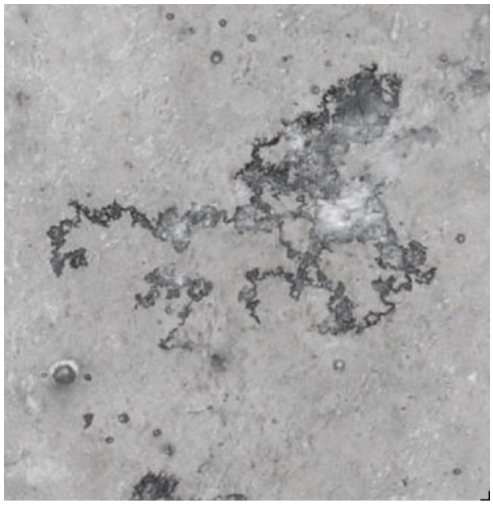

Figure 8. Filiform corrosion of AZ31B-H24
after 72-h NSF (6X).

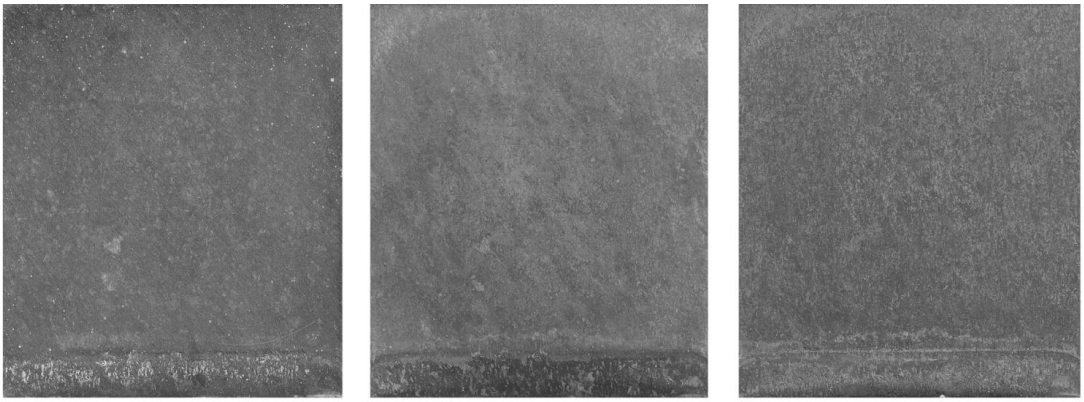

Figure 9. GM 9540P cyclic corrosion of AZ31B-H24 at 1, 5, and 10 cycles.

3.4 AZ91C

This particular alloy exhibited the lowest mass loss and cosmetic corrosion attributes among all of the alloys in this study. Similar to AZ31B-H24, the main alloying element in AZ91C is Al, though in significantly higher amounts. This alloy is popularly used for aerospace castings but is not used for structural applications due to its low inherent as-cast strength. The cosmetic damage from corrosion observed was less than typically observed for some Al alloys. For instance, it matched AA5083-H131 in appearance for similar exposure durations under NSF and cyclic and easily outperformed AA2024-T3 under those same conditions. Figures 10 and 11 illustrate the near complete lack of corrosion for this alloy under NSF and cyclic exposures.

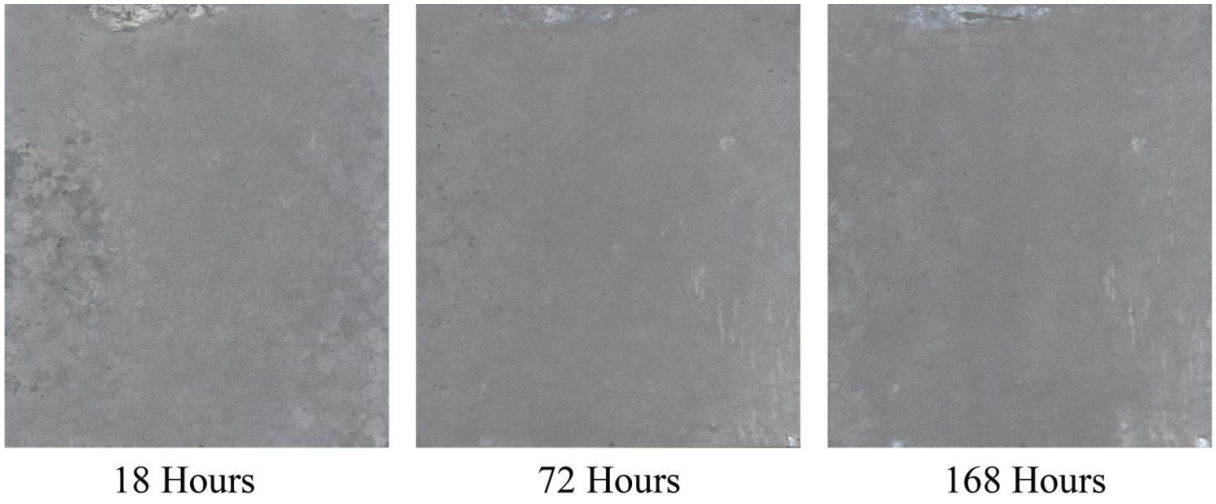

Figure 10. AZ91C after NSF.

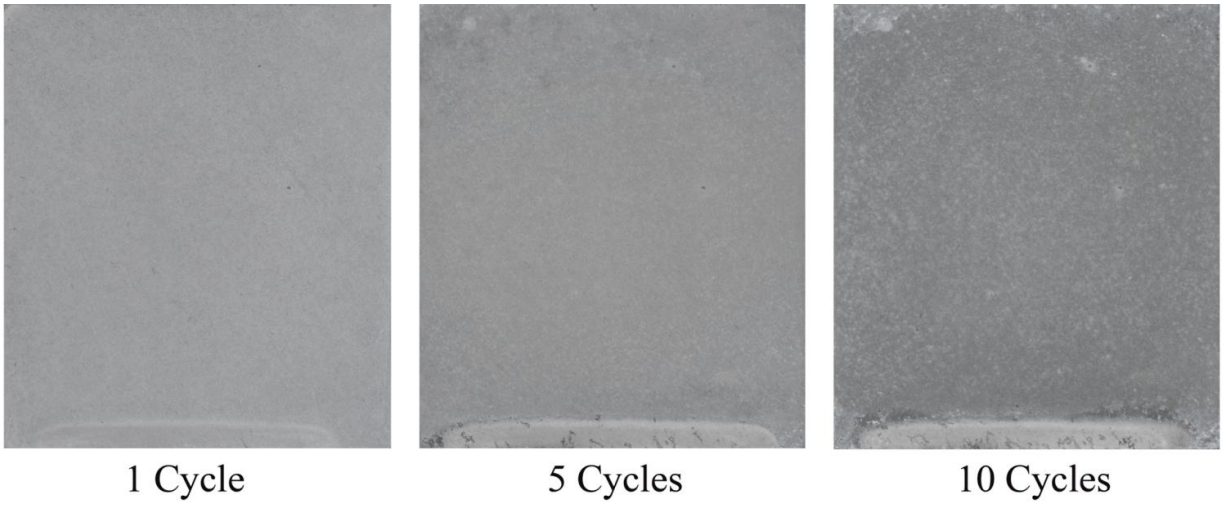

Figure 11. AZ91C after GM 9540P cyclic corrosion.

3.5 EV31A

The EV31A alloy, also known commercially as Elektron 21 or E21 is a cast alloy produced by Magnesium Elektron (*20*). It is well known for its excellent mechanical properties and corrosion resistance and appears in SAE Aerospace Material Specification AMS4429 (*21*). Similar to WE43, it contains rare earth alloying additions though overall in lower concentration. Its composition is based upon zirconium and zinc additions with neodymium, gadolinium, and small amounts of other rare earths. The mass loss values determined under accelerated methods were quite low and generally fell between values observed for AZ31B and WE43. Most discolorations observed under NSF and cyclic were from staining; however, the actual corrosion produced under NSF on EV31A consisted of very deep (greater than 100 µm) but localized elongated pits. Figures 12–14 depict the corrosion of EV31A and include a close-up of the localized pitting morphology produced under NSF in figure 13.

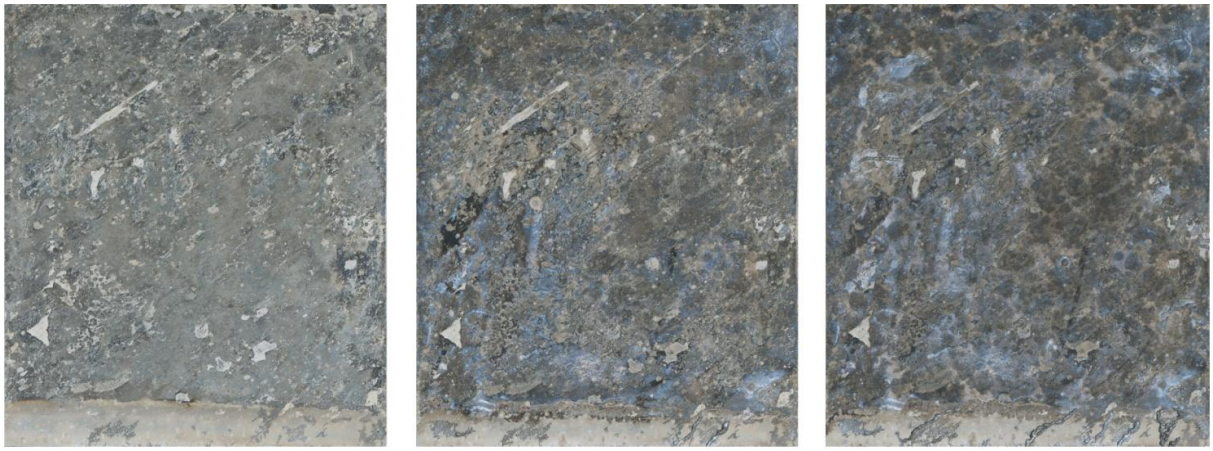

Figure 12. EV31A after NSF.

(a) **(b)**

Figure 13. Corrosion of EV31A localized pits after 168-h NSF (6X) as corroded (a) and after cleaning (b).

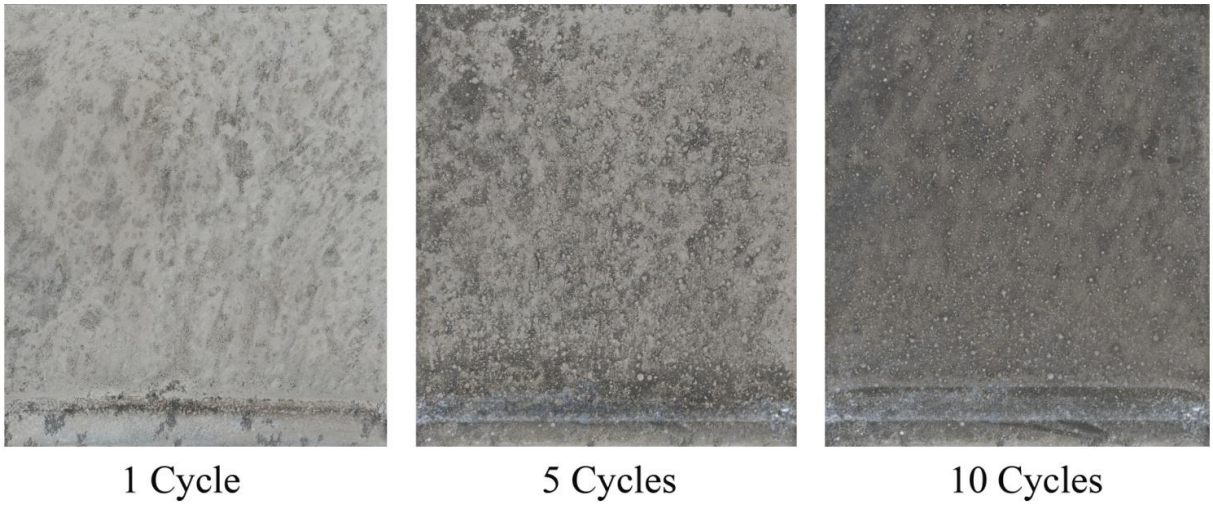

Figure 14. EV31A after GM 9540P cyclic corrosion.

3.6 WE43B-T5

Mg alloy WE43B is best known for relatively good corrosion resistance and good mechanical properties, making it a prospective candidate for plates. It is used in commercial and military aviation applications and has demonstrated good flame resistance (*22*). For this study. the wrought form of WE43B (T5) was exposed. It shared similar corrosion resistance in the exposures as AZ31B-H24 and EV31A. The mode of corrosion for this alloy was similar that of AZ31B, with dark staining and diffuse pitting. There was little or no filiform corrosion observed. The NSF and cyclic scans for WE43B-T5 are displayed in figures 15 and 16.

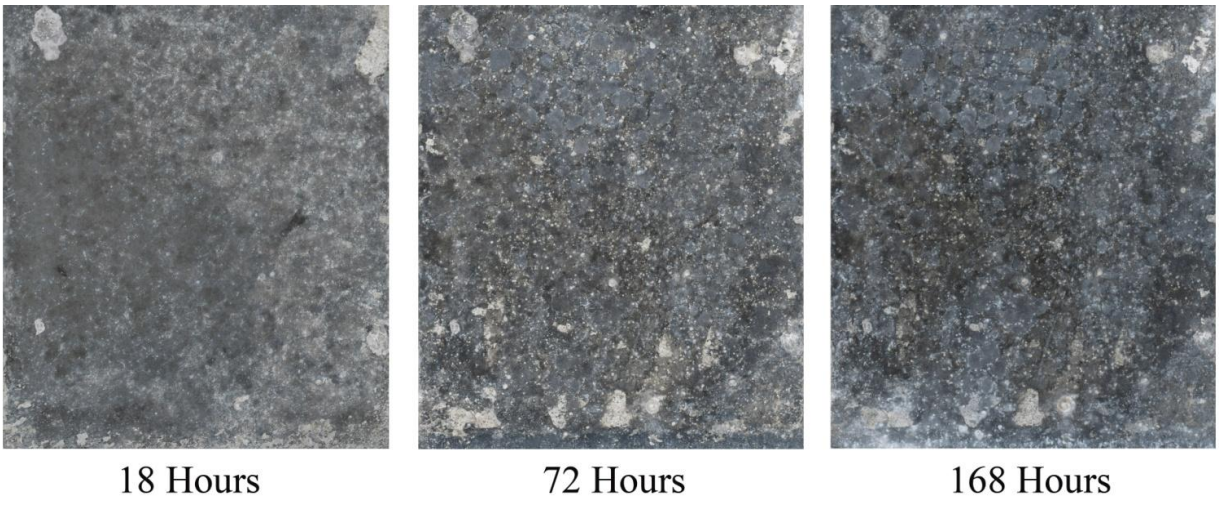

Figure 15. WE43B-T5 after NSF.

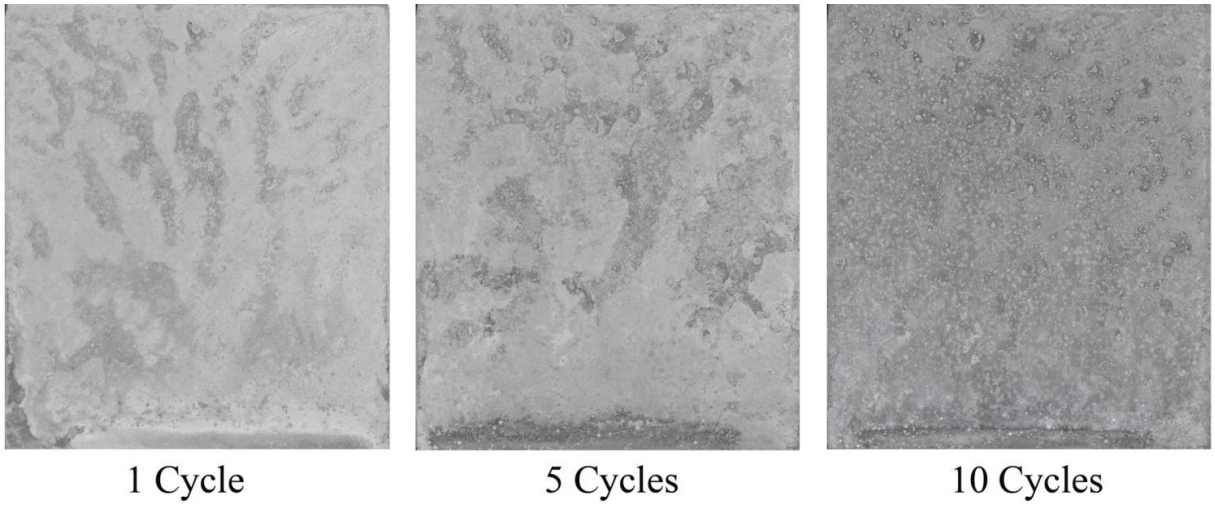

Figure 16. WE43B-T5 after GM 9540P cyclic corrosion.

3.7 ZAXE1711

Extruded ZAXE1711 is the second alloy in this study produced in Japan using the SWAP powder extrusion method. From an alloy composition standpoint, it resembles an AZ61 type alloy with additions of calcium and lanthanum. It is marginally stronger than AMX602 and has slightly better ballistic response (*23*). Results for corrosion resistance were better than AZ31B under cyclic corrosion but had about the same or slightly lower performance than AZ31B under NSF. The corrosion observed under NSF and cyclic exposures in figures 17 and 18 was mainly filiform attack and dark staining with little to no pitting. The cyclic was less severe than the NSF.

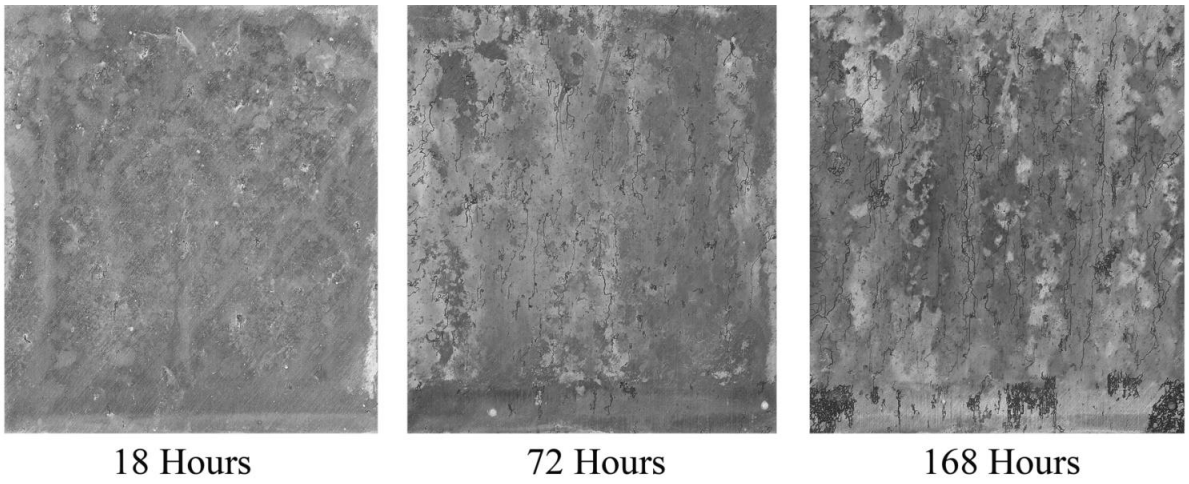

Figure 17. NSF corrosion of ZAXE1711-D at 18, 72, and 168 h.

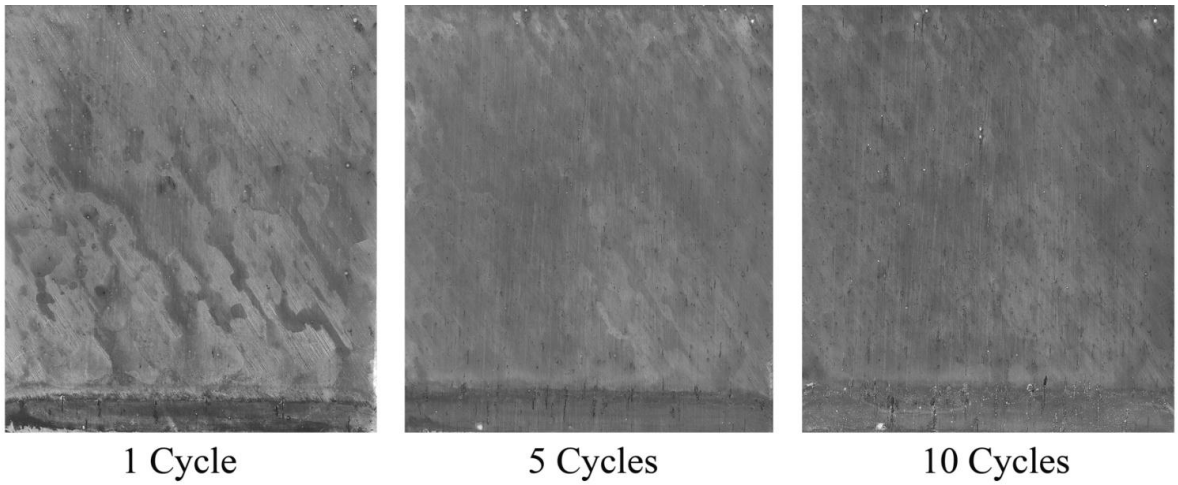

Figure 18. GM 9540P cyclic corrosion of ZAXE1711-C at 1, 5, and 10 cycles.

3.8 ZE41A

Mg alloy ZE41A has been used for decades in military and commercial aviation systems. It is best known in the U.S. Army for its use by Sikorsky in UH-60 Blackhawk transmission housings and has long been known for issues with corrosion and under this application in particular (*24–29*). In both NSF and cyclic corrosion exposure, the ZE41A indeed corroded more severely that the other alloys though not nearly as much as the CP Mg. As with CP Mg under NSF, the corrosion was very active and necessitated additional imaging from the earlier 4- and 8-h observations. The NSF damage to this alloy was characterized by extremely deep pits extending well into within the bulk of the specimen. This extensive pitting was the main mechanism for the appreciable mass loss measurement. In addition to somewhat milder pitting compared with NSF, the cyclic specimen also showed traces of filiform attack. Good images of the pitting and the mixed mode corrosion are displayed in figures 19 and 20.

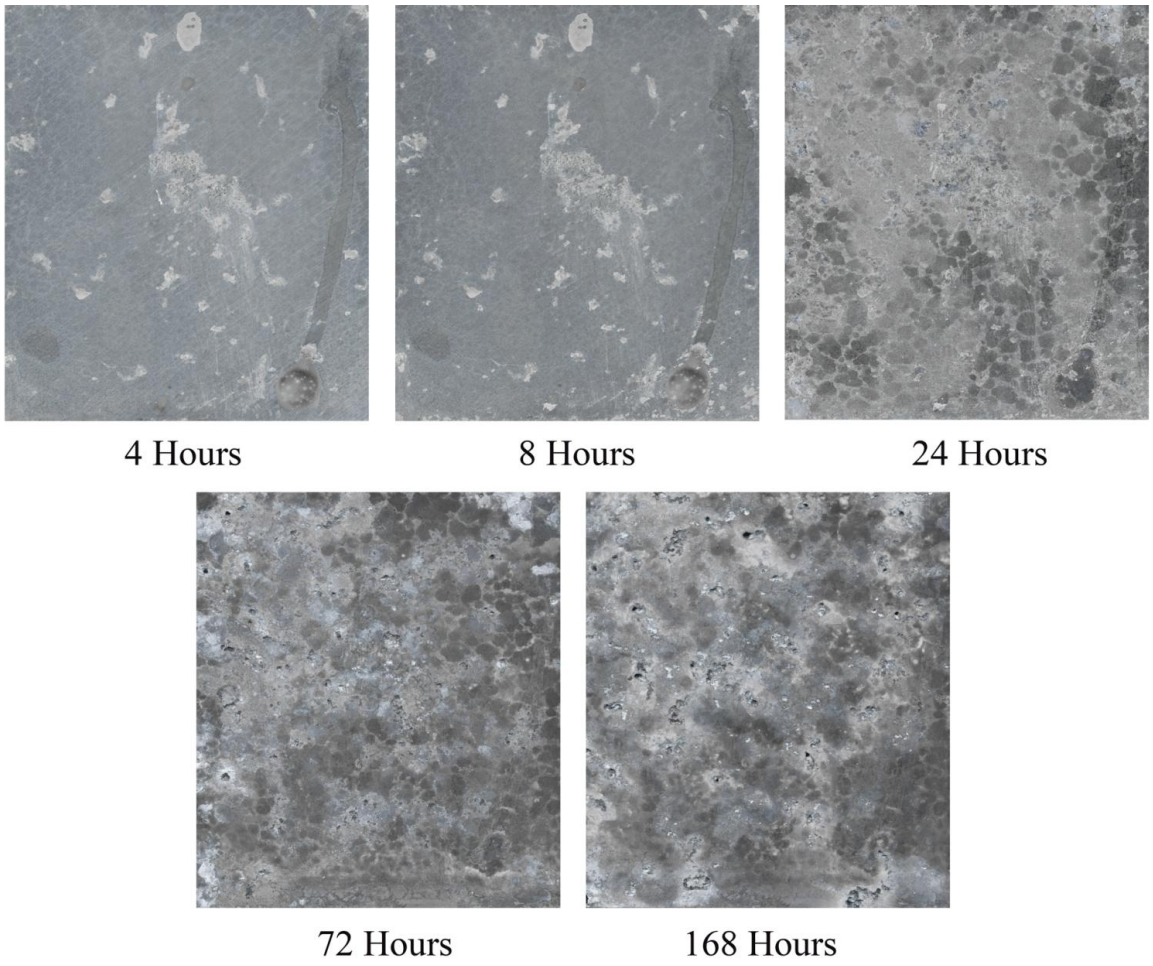

Figure 19. ZE41A after NSF.

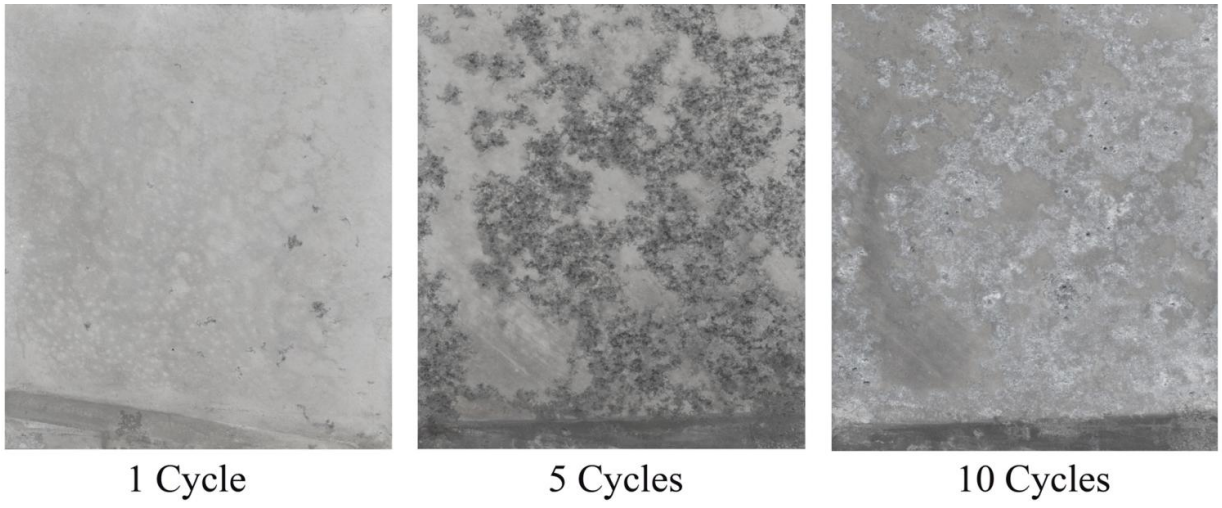

Figure 20. ZE41A after GM 9540P cyclic corrosion.

3.9 Accelerated Corrosion Rate Determinations

Mass loss values for the alloys in NSF and GM 9540P cyclic corrosion were collected and the resultant corrosion rates in mils per year were calculated and plotted in figure 21. The overall corrosion rates were determined using mass loss and because the mass loss occurred from corrosion attack on all surfaces, post cleaning scans for the front and also of the backsides of the NSF and cyclic corrosion specimens were acquired and are displayed in figures 22–25.

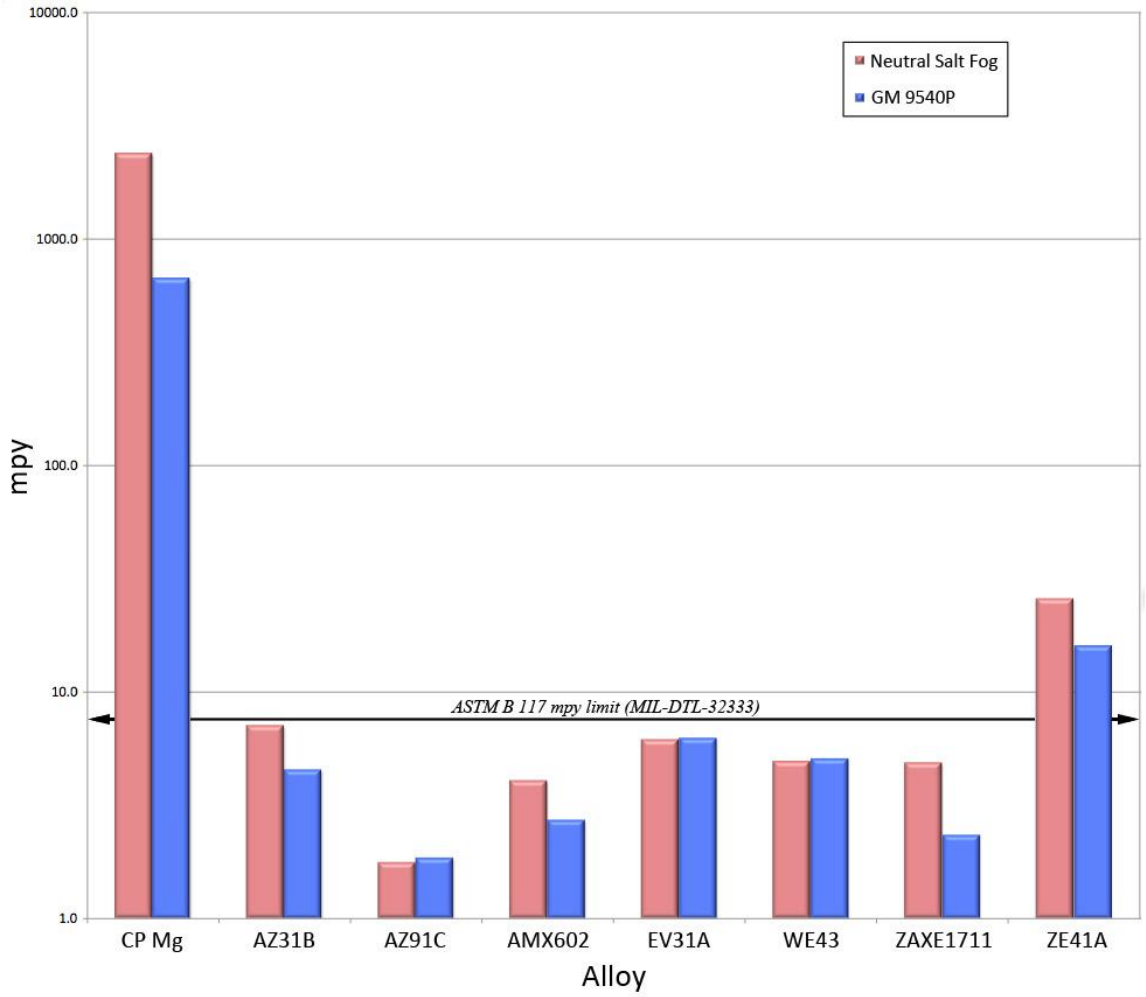

Figure 21. Corrosion rates in mils per year based upon mass loss measurements after NSF (red) and GM 9540P cyclic corrosion exposures (blue).

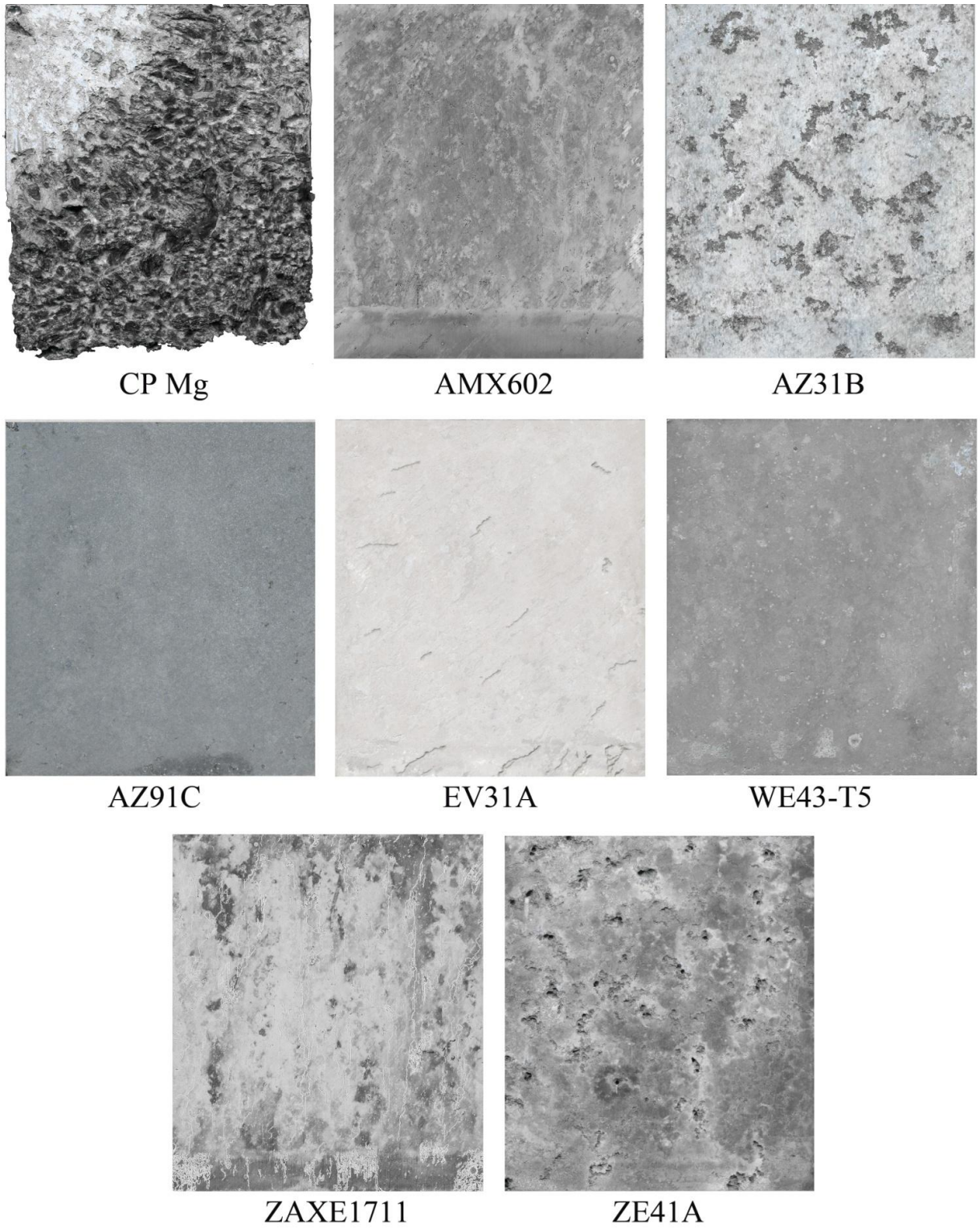

Figure 22. Front sides of 168-h NSF specimens after cleaning to reveal extent of substrate loss.

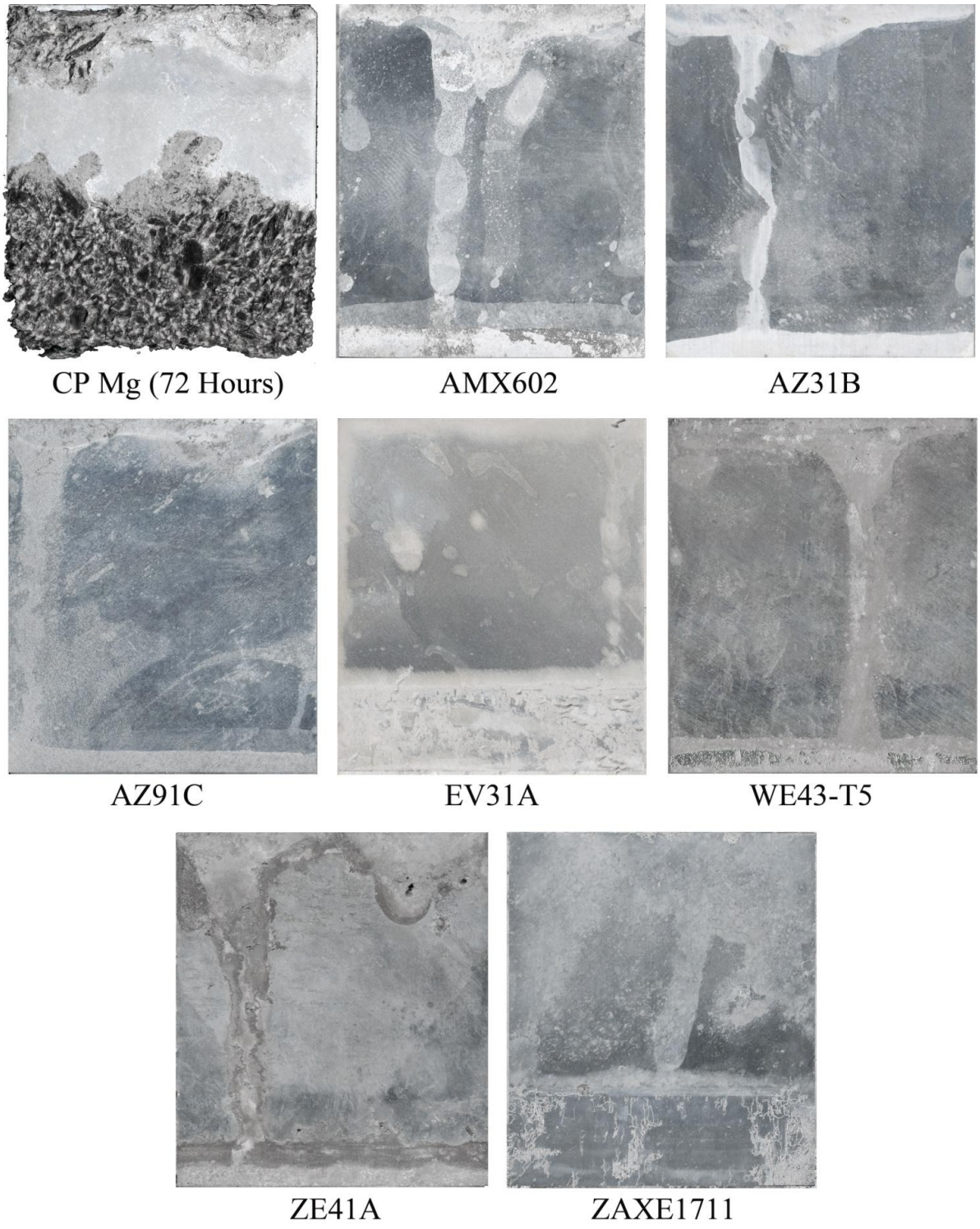

Figure 23. Rear sides of 168-h NSF specimens after cleaning to reveal extent of substrate loss.

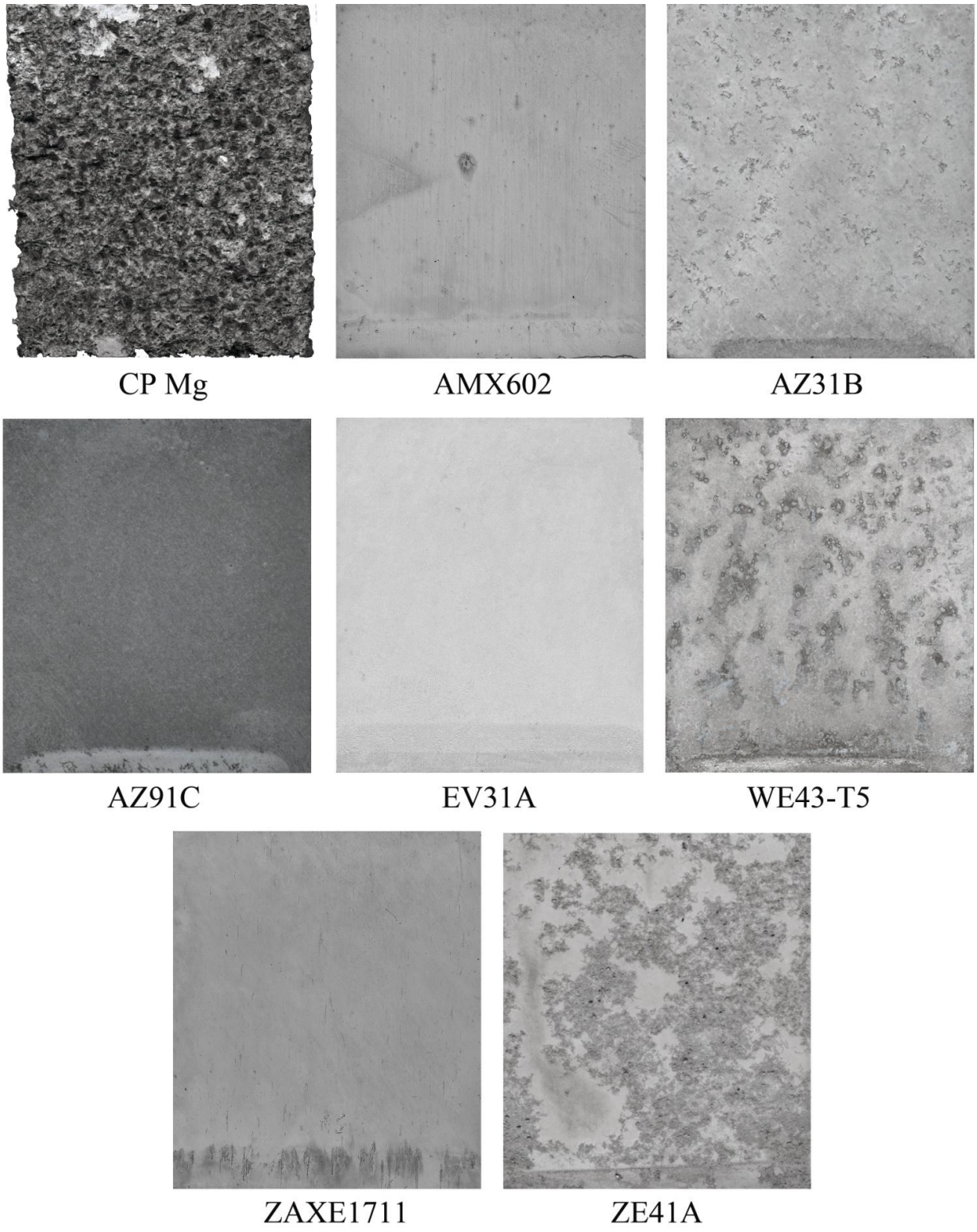

Figure 24. Front sides of 10-cycle GM 9540P cyclic corrosion specimens after cleaning to reveal extent of substrate loss.

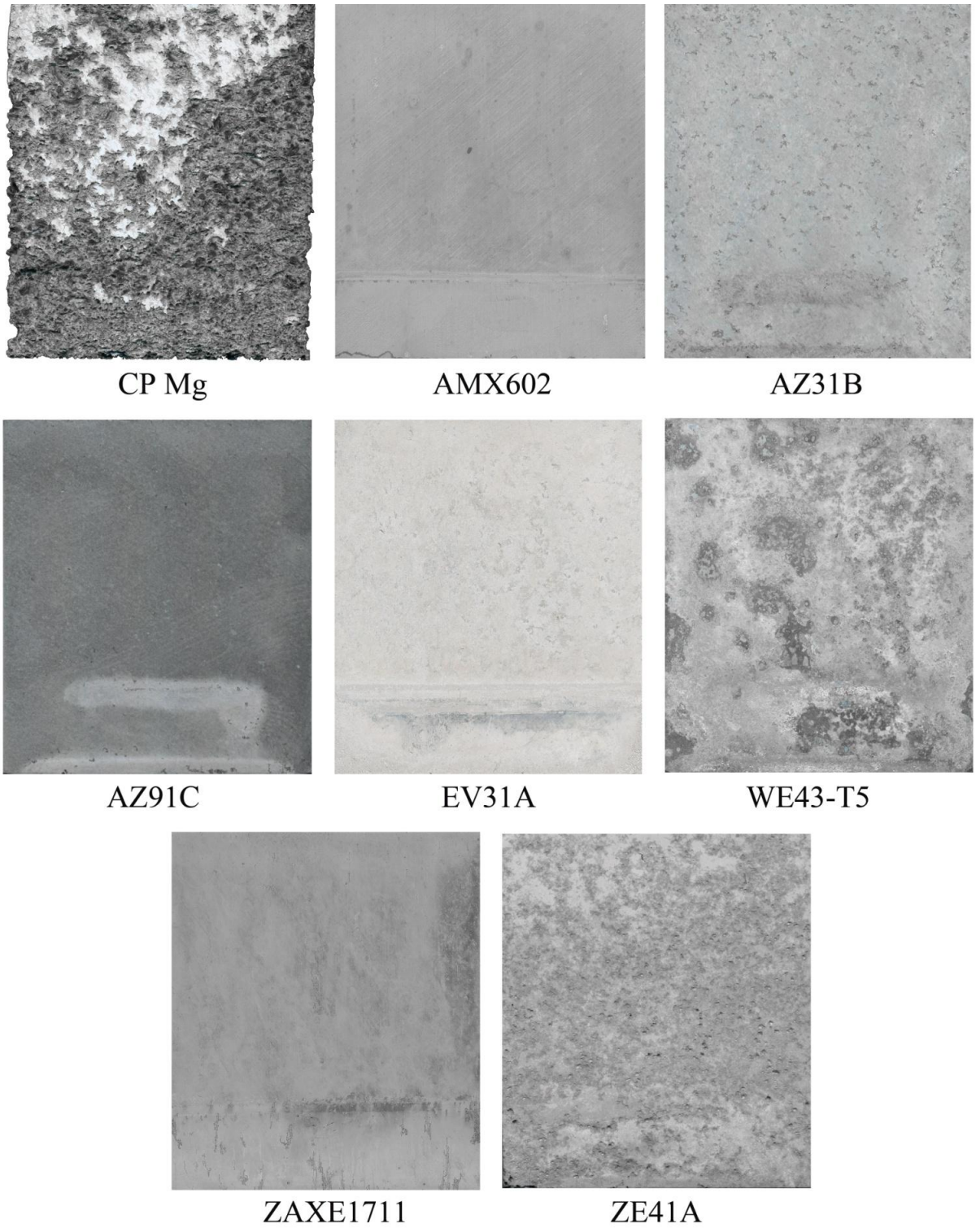

Figure 25. Rear sides of 10-cycle GM 9540P cyclic corrosion specimens after cleaning to reveal extent of substrate loss.

3.10 Electro-chemical Behavior

To better understand Mg alloy corrosion at a more fundamental level, the electro-chemical behavior of a metal or alloy is often studied. Specifically, potentiodynamic polarization provides a methodology to relate the OCP of an alloy (E_{corr}) to the corrosion current density (I_{corr}). Figure 26 shows this relationship between E_{corr} and I_{corr} for all of the alloys reported in this study.

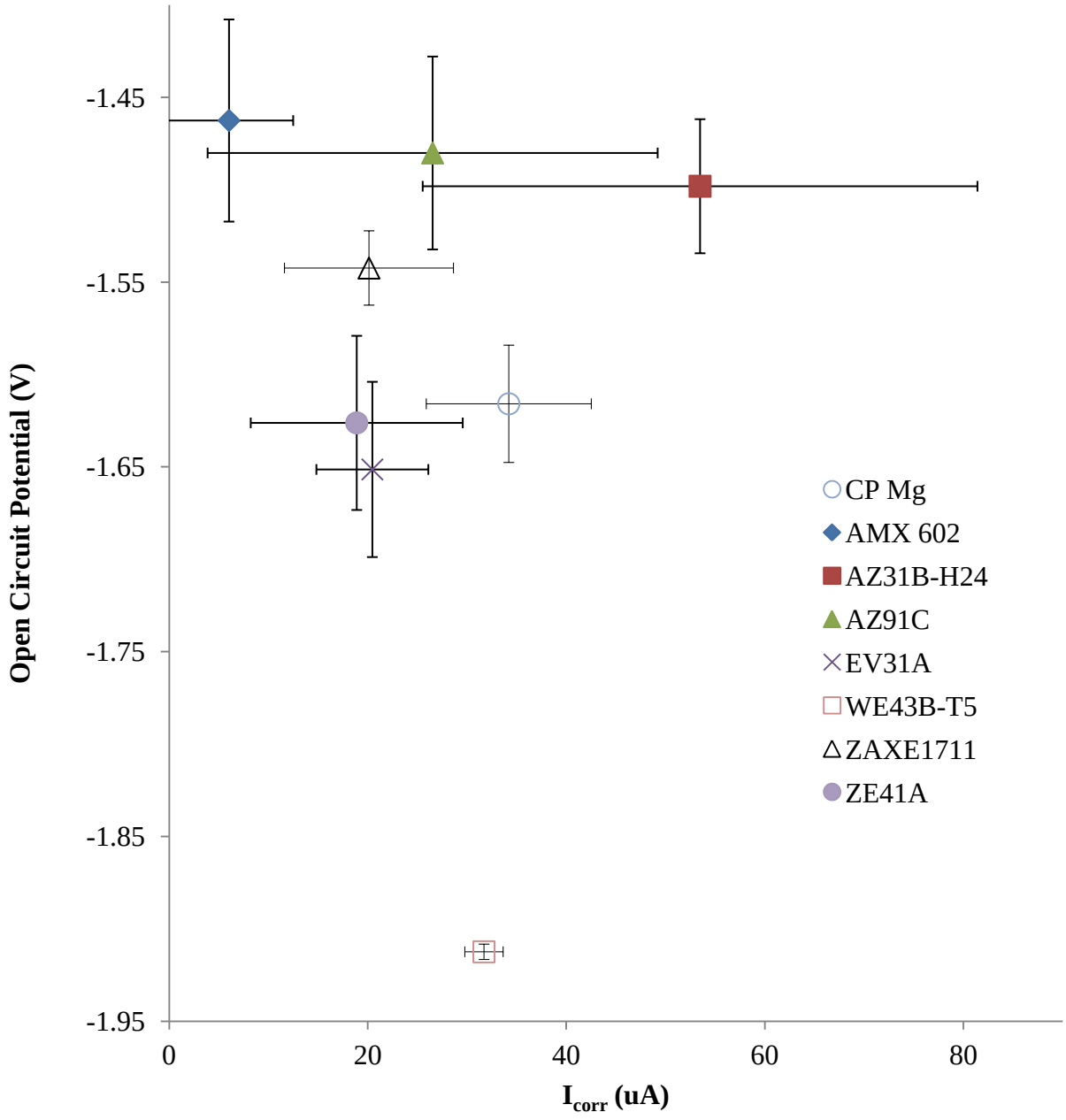

Figure 26. Potentiodynamic polarization analysis of Mg alloys.

Results from this type of analysis are not always in agreement with what is observed using more qualitative approaches such as NSF, cyclic corrosion exposure, or outdoor exposure, and the reasons for this disagreement are not trivial. Frankel (*30*) provides some insight into the discrepancy between corrosion rates calculated from electro-chemical data and rates determined from mass loss measurement. One example of such discrepancies in our data can be seen by comparing the mass loss data for EV31A and ZE41A with the electro-chemical data for the two alloys. Clearly, the mass loss data show EV31A meeting the 7-mpy mass loss limit for Mg alloys to be used by the DOD for ballistic purposes, whereas ZE41A corrodes at a rate of approximately one order of magnitude faster and does not meet the corrosion requirements to be incorporated into the ballistic performance specification (*6*). Potentiodynamic polarization suggests that these alloys would corrode at near equivalent rates because of similar corrosion current densities (figure 26). The electro-chemical data will be discussed in the following section.

4. Discussion

Corrosion will always remain a consideration for Mg alloys just as it is for many other materials. However, designers considering Mg-based materials are now better informed of the galvanic and general corrosion issues. Higher-purity alloys limiting iron (Fe), cobalt (Co), nickel (Ni), and copper (Cu) contaminants have significantly improved corrosion resistance. Modern methods limiting direct Mg substrate contact with corrosive environments include electro-chemical plating, conversion coatings, anodizing, vapor-phase deposition techniques, laser surface alloying/cladding, and organic coatings (*31*). Coating solutions applied in clean environments with robust process controls such as Tagnite* anodizing, plasma gel anodizing, and Gardobond† X4729 composite coating have provided superior corrosion, abrasion, and wear resistance (*32*). Since 1996, the Tagnite coating process has protected Mg components on the U.S. Navy's Sikorsky CH-53 Sea Stallion helicopter, the U.S. Air Force F-22 Raptor fighter, U.S. Marine Corps Expeditionary Force Vehicle prototypes, and the U.S. Army's Boeing Apache helicopter. Novel repair techniques have also been recently developed to address corrosion in fielded systems. For instance, cold-spray technology developed at the U.S. Army Research Laboratory has been a cost-effective and technically feasible solution for field repair and surface protection of corrosion damaged Mg components (*33*). In addition to alloy design and coatings, engineers now mitigate corrosion through proper joint design, insulation of dissimilar metals, manufacturing process controls, and appropriate maintenance schedules.

* Tagnite is a registered trademark of Technology Applications Group Inc., Atlanta, GA.

† Gardobond is a registered trademark of Trakehner Straße 3, Frankfurt am Main, Germany.

While significant corrosion damage resulted in the accelerated exposure experiments on substrates such as CP Mg and ZE41A, other alloys such as AZ91C and the SWAP-prepared alloys experienced little to almost no corrosion damage. This result provides evidence that supports ongoing research and development aimed at corrosion-resistant Mg alloys with a higher degree of corrosion resistance. For the accelerated corrosion procedures, there was reasonable agreement of overall alloy trends (figure 21) between the NSF and the GM 9540P cyclic corrosion procedures. The largest variations occurred among the SWAP-prepared alloys where greater relative gaps in mils per year between NSF and cyclic corrosion experiments were evident. The sampling size was small due to a lack of material; therefore, standard error bars were not generated for the mass loss. For NSF exposure, the order of corrosion resistance calculated from mass loss from highest to lowest was AZ91C, AMX602, ZAXE1711, WE43B, EV31A, AZ31B, ZE41A, and CP Mg. For the GM 9540P cyclic corrosion, the order of corrosion resistance based on mass loss in mils per year was AZ91C, ZAXE1711, AMX602, AZ31B, WE43B, EV31A, ZE41A, and CP Mg. The corrosion damage on the EV31A was very interesting. The overall mass loss for this alloy was low but the deep localized damage that did occur from pitting under NSF suggests the possible presence of tramp elements such as Fe, Ni, or Cu, or intermetallic phases that act either as local cathodes or anodes. Were it not for this localized attack, the EV31A have visually resembled AZ91C. If this localized attack can be eliminated or reduced, the cast alloy EV31A would be worthy of further development as a wrought plate product.

The corrosion resistance of AZ91C was surprising. The visual evidence of corrosion or lack of it resembled highly corrosion-resistant 5000-series Al alloys, such as AA5083. The high level of corrosion resistance is visible in figure 27, comparing alloy AZ91C with Al-series alloys AA5083-H131 (*34*, *35*) and AA2024-T3 (*36*) at 168 h of NSF.

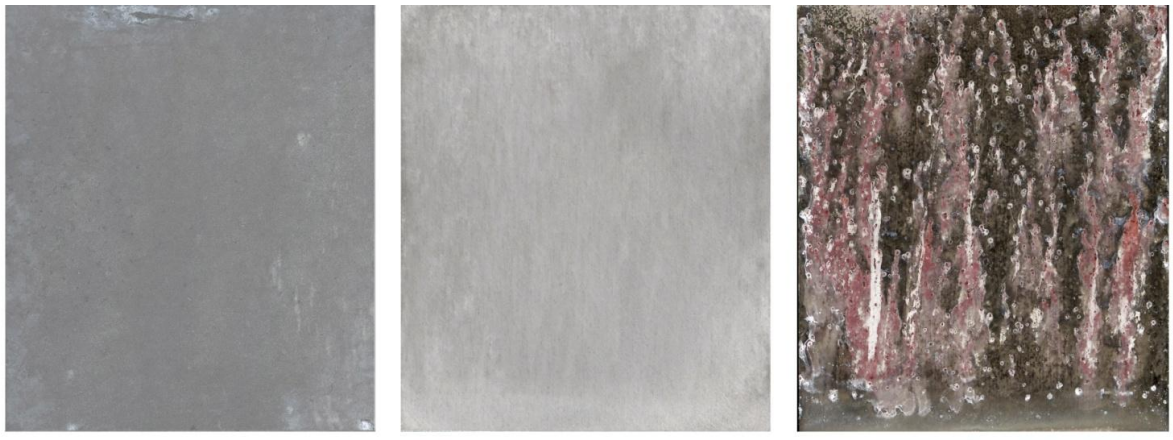

Figure 27. 168-h NSF comparisons of (a) AZ91C-T6, (b) Al 5083-H131, and (c) Al 2024-T3.

Similarly, figure 28 compares the same three alloys at 10 cycles of GM 9540P.

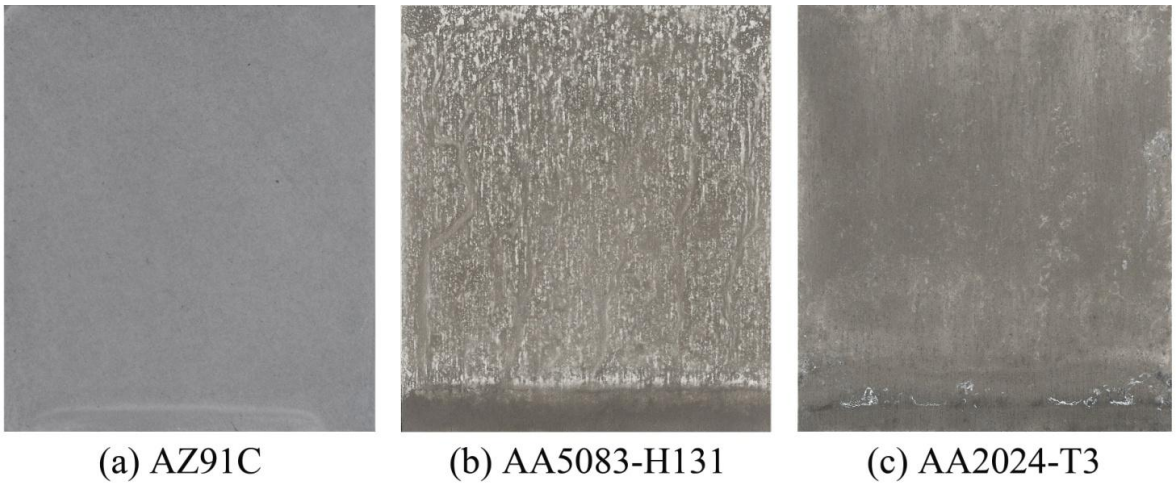

Figure 28. 10-cycle GM 9540P cyclic corrosion comparisons of (a) AZ91C, (b) Al 5083-H131, and (c) Al 2024-T3.

Unexpectedly, the performance of this batch of alloy was beyond typical AZ91C. Personal communications with Magnesium Elektron regarding this high resistance to corrosion suggested that the material sold as AZ91C, from which the samples originated, may have actually been AZ91E (*11*). The AZ91E alloy is similar to AZ91C but has much tighter controls on the permitted concentrations of harmful impurity elements such as Fe, Ni, and Cu. A formal certification of composition (*37*) for this particular sample stock was obtained through the U.S. Navy Air Warfare Center and is listed in table 5. A close examination of the AZ91C constituents confirms low concentrations of silicon, Cu, and Ni, all factors that greatly improve corrosion resistance.

Table 5. Chemical certification/analysis for AZ91C.

Element (%)							
Aluminum	**Manganese**	**Zinc**	**Silicon**	**Copper**	**Nickel**	**Others Each**	**Magnesium**
8.25	0.26	0.64	0.04	<0.01	<0.002	<0.30	REM

The electro-chemical measurements on the Mg alloys evaluated in this research provide a guideline for estimating the susceptibility of each alloy to corrosion. Based on these measurements, alloys with the lowest corrosion current density are expected to be the most resistant to corrosion, and those with the highest E_{corr} are expected to resist galvanic corrosion when coupled to a slightly more noble metal. The data in figure 26 suggest that all of the alloys in this research will corrode at about the same rate based on the I_{corr}. Some alloys such as AZ31B, AZ91, and AMX602 may exhibit somewhat stable galvanic behavior when coupled to lightweight Al alloys. Certainly, further study is necessary to evaluate the corrosion behavior of these Mg alloys when coupled to more noble other metals. Although there was no exact correlation between electro-chemical experiments and mass loss data, alloys with the highest

open circuit potential (AMX602, ZAXE1711, AZ91C, and AZ31B) did have good corrosion resistance in accelerated corrosion experiments. The SWAP-produced alloys also had a smaller range of corrosion current density compared with the AZ-series alloys. Electro-chemically, CP Mg, ZE41A, and EV31A had similar E_{corr} and I_{corr}; however, accelerated corrosion testing showed EV31A to have minimal mass loss in these tests. Perhaps the mass loss of EV31A happens rapidly and early in accelerated corrosion testing followed by a passivation. Polarization curves of EV31A show a slight passivation occurring in some curves just above the OCP. Research into this passive region and the surprisingly low E_{corr} and I_{corr} of WE43 is ongoing.

While the improved corrosion resistance of Mg alloys is indeed encouraging, the designers must not become complacent regarding their selection of what other materials are selected for contact with the Mg alloy. Designers must not forget that Mg is anodic to every other metallic material available for engineering design. A specific and extreme example of poor design decision would be the use of graphite in contact with Mg; similar to Mg, it is very lightweight and is very strong as a composite. The temptation can therefore be very great to use the two materials together in the design of new systems. The galvanic series (*38*) for metals, in figure 29, shows a voltage gap of nearly 2 V between Mg and graphite and clearly highlights the need for vigilance on the part of designers with regards to materials selection in conjunction with Mg alloys.

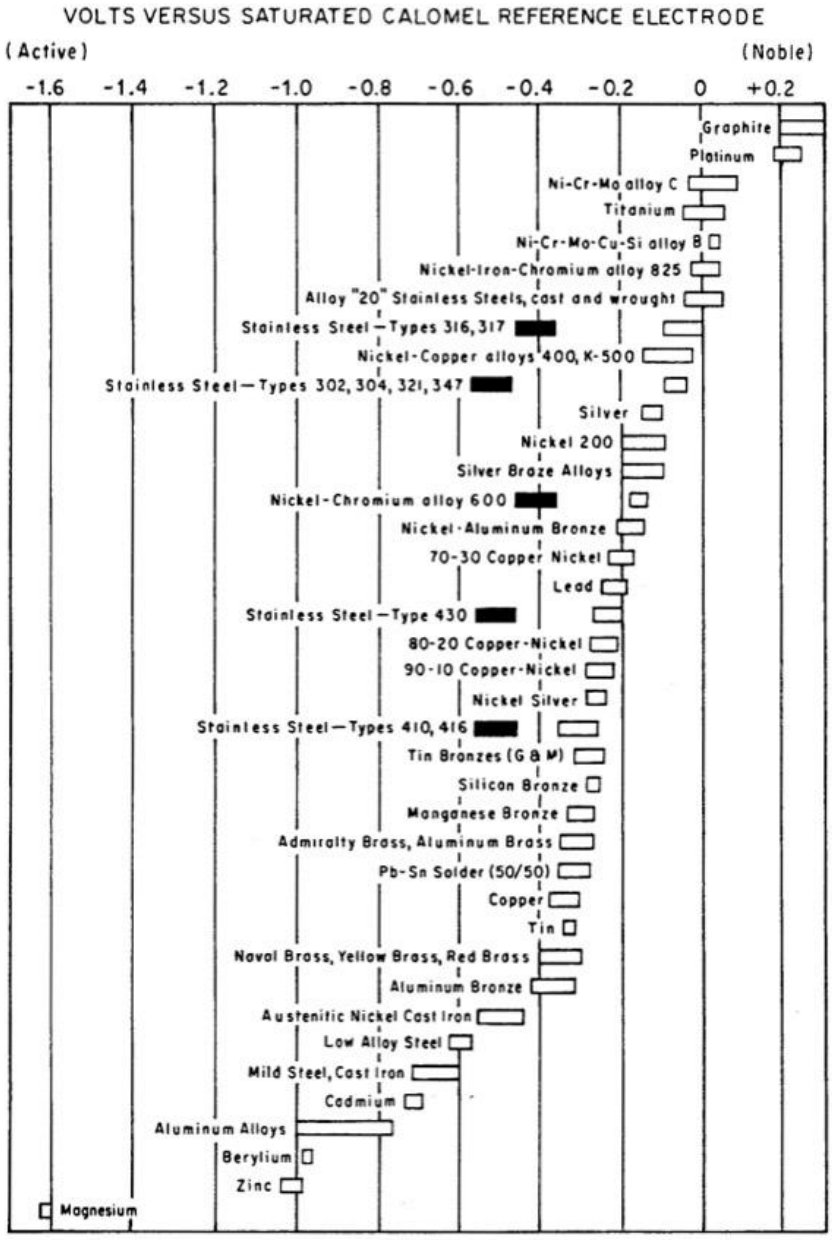

Figure 29. Galvanic series showing approximately 1.8-V gap between Mg and graphite with other metallic materials between (*37*, *38*) (Reprinted, with permission, from ASTM G82-98 (2014) Standard Guide for Development and Use of a Galvanic Series for Predicting Galvanic Corrosion Performance, copyright ASTM International, 100 Barr Harbor Drive, West Conshohocken, PA 19428. A copy of the complete standard may be obtained from ASTM International, http://www.astm.org.

Increased corrosion resistance of alloys such as AZ31B-H24, AZ91C-T6, WE43B-T5, EV31A, and the SWAP-produced alloys, are encouraging signs of increasing quality, research, and innovation directed at a wide variety of lightweight and durable products and applications. It is

the responsibility of design engineers to ensure safety and environmental robustness of Mg-based products through proper materials selection and electrical and moisture isolation of the Mg from all dissimilar metals.

5. Conclusions

- Overall, there was good agreement between the NSF and GM 9540P in the order of the mpy performance of the very best and the very worst of the alloys; however, results were mixed amongst the intermediate performing alloys.
- The excellent performance of the AZ91C-T6 was most likely due to a no-cost “upgrade” to AZ91E-T6.
- Avoidance of Fe, Co, Ni, and Cu, as seen in the AZ91C-T6, results in significantly improved corrosion resistance and is a good practice to follow for other Mg alloys.
- In addition to AZ31B, the rare-earth-based alloys EV31A and WE43 exhibit a good balance of corrosion resistance and mechanical properties.
- The SWAP-produced alloys AMX602 and ZAXE1711 provided encouraging results both mechanically and for corrosion resistance. Further studies and development of up-scaled plates are encouraged.

6. References

1. ASTM B117-90. Standard Method of Salt Spray (Fog) Testing. *Annu. Book ASTM Stand.* **1990**.
2. General Motors (GM) Standard 9540P. Accelerated Corrosion Test. General Motors Engineering Standards **1997**.
3. Mathaudhu, S.; Nyberg, E. Magnesium Alloys in Army Applications: Past Current and Future Solutions. *Proceedings of the Minerals, Metals and Materials (TMS) Annual Symposium*, Seattle, WA, 2010.
4. 2017 and Later Model Year Light-Duty Vehicle Greenhouse Gas Emissions and Corporate Average Fuel Economy Standards. *Federal Register* **2012,** *77* (199), Book 2, pp 62623–63200.
5. Jones; T. DeLorme, R.; Burkins, M.; Gooch, W. *Ballistic Evaluation of Magnesium Alloy AZ31B;* ARL-TR-4077; U.S. Army Research Laboratory: Aberdeen Proving Ground, MD, April 2007.
6. Jones, T.; Burkins, M.; Gooch, W. *An Analysis of Magnesium Alloy AZ31B-H24 for Ballistic Applications;* ARL-TR-4327; U.S. Army Research Laboratory: Aberdeen Proving Ground, MD, December 2007.
7. Jones, T.; DeLorme, R. *Development of a Ballistic Specification for Magnesium Alloy AZ31B;* ARL-TR-4664; U.S. Army Research Laboratory: Aberdeen Proving Ground, MD, December 2008.
8. MIL-DTL-32333. *Armor Plate, Magnesium Alloy, AZ31B, Applique* **2009**.
9. Jones T.; Placzankis, B. *The Ballistic and Corrosion Evaluation of Magnesium Elektron E675 vs. Baseline Magnesium Alloy AZ31B and Aluminum Alloy 5083 for Armor Applications;* ARL-TR-5565; U.S. Army Research Laboratory: Aberdeen Proving Ground, MD, June 2011.
10. *Magnesium Alloy Castings, Sand 2.8Nd - 1.4Gd - 0.4Zn - 0.6Zr (EV31A - T6) Solution and Precipitation Heat Treated, Revision A;* AMS4429; SAE International: Warrendale, PA, May 2012.
11. Placzankis, B.; Miller, C.; Mathaudhu, S.; DeLorme, R. *Corrosion Comparisons Among Magnesium Alloys of Interest for DOD Systems Using Laboratory Based Accelerated Corrosion Methods;* Paper No. 10085; National Association of Corrosion Engineers (NACE) International: Houston, TX, 2010.

12. ASTM B92/B92M-07. Standard Specification for Unalloyed Magnesium Ingot and Stick for Remelting. *Annu. Book ASTM Stand.* **2007**.

13. Jones, T.; Kondoh, K. *Initial Evaluation of Advanced Powder Metallurgy Magnesium Alloys for Armor Development;* ARL-TR-4828; U.S. Army Research Laboratory: Aberdeen Proving Ground, MD, May 2009.

14. ASTM B90/B90M-07. Standard Specification for Magnesium-Alloy Sheet and Plate. *Annu. Book ASTM Stand.* **2007**.

15. ASTM B80-07. Standard Specification for Magnesium-Alloy Sand Castings. *Annu. Book ASTM Stand.* **2007**.

16. Jones,T.; Labukas, J.; Placzankis, B. Corrosion and Ballistic Analysis of New Military Grade Magnesium Alloys AMX602 and ZAXE1711 for Armor Applications. DOD Corrosion Conference 2011, La Quinta, CA, 31 July–5 August 2011.

17. Miller, C.; Placzankis, B.; Kidd, J.; Luckner, J. *Assessment of Aviation Coating Systems Performance Using Accelerated Test Methods;* ARL-TR-3428; U.S. Army Research Laboratory: Aberdeen Proving Ground, MD, February 2005.

18. ASTM G97 - 97(2007). Standard Test Method for Laboratory Evaluation of Magnesium Sacrificial Anode Test Specimens for Underground Applications. *Annu. Book ASTM Stand.* **2007**.

19. Fontana, M. G. *Corrosion Engineering*; McGraw-Hill: New York, 1986; p 14.

20. Magnesium Elektron North America. http://www.magnesium-elektron.com/ (accessed May 2006).

21. *Magnesium Alloy Castings, Sand 2.8Nd - 1.4Gd - 0.4Zn - 0.6Zr (EV31A - T6), Solution and Precipitation Heat Treated;* SAE Aerospace Material Specification AMS4429; Society of Automotive Engineers International: Warrendale, PA, 2012.

22. Marker, T. Task Group Session on New Flammability Test for Magnesium-Alloy Seat Structure. International Aircraft Materials Fire Test Working Group Meeting, Singapore, June 2012.

23. Jones, T.; Kondoh, K. Ballistic Analysis of New Military Grade Magnesium Alloys for Armor Applications. *Proceedings of the Minerals, Metals and Materials (TMS) Annual Symposium*, San Diego, CA, February 2011.

24. Champagne, V.; Leyman, P. Helfritch, D. *Magnesium Repair by Cold Spray;* ARL-TR-4438; U.S. Army Research Laboratory: Aberdeen Proving Ground, MD, May 2008.

25. Kelley, J. *Assessment of Some Chromated and Non-Chromated Primers on Magnesium ZE41A, Aluminum 2024, and Steel 4340 via Electro-Chemical Impedance Spectroscopy;* ARL-TR-3290; U.S. Army Research Laboratory: Aberdeen Proving Ground, MD, August 2004.

26. Chang, F.; Huie, R.; Placzankis, B. Assessment of Some Advanced Protective Schemes, Including Chromate and Non-Chromate Conversion Coatings for Mg Alloy ZE41A-T5 Using Electro-Chemical Impedance Spectroscopy. *Proceedings of the 1994 Tri-Service Conference on Corrosion*, Orlando, FL, July 1994; pp 549–564.

27. Levy, M.; Chang, F.; Placzankis, B.; Huie, R. *Improved Protective Schemes on Magnesium Aircraft Alloys;* NACE Paper no. 617; Corrosion 1994 Conference, Baltimore, MD, 1994.

28. Levy, M.; Bombard, R.; Huie, R. *Assessment of Some Corrosion Protection Schemes for Magnesium Alloy ZE41A;* MTL-TR-89-9; U.S. Army Laboratory Command: Aberdeen Proving Ground, MD, February 1989.

29. Gallaccio, A.; Ebihara, W. *Corrosion Susceptibilities of Magnesium Alloys AZ91, EZ33, and ZE41;* ARSCD-TR-83007; U.S. Army Armament Research and Development, Command Fire Control and Small Caliber Weapons Systems Laboratory: Dover, NJ, 1983.

30. Frankel,G. S. Electro-Chemical Techniques in Corrosion: Status, Limitations, and Needs. *Journal of ASTM International* **2008,** *5* (2), 1–27.

31. Ostrovsky, I. Henn, Y. Present State and Future of Magnesium Application in Aerospace Industry. Presented at ASTEC 2007 International Conference–New Challenges in Aeronautics, Moscow, Russia, 19–22 August 2007.

32. Gray, J. E.; Luan, B. Protective Coatings on Magnesium and its Alloys–A Critical Review. *Journal of Alloys and Compounds* **2002,** *336* (1-2), 88–113.

33. Champagne, V. K. The Repair of Magnesium Rotorcraft Components by Cold Spray. *Journal of Failure Analysis and Prevention* **2008,** *8* (2), 164–175.

34. *Aluminium Alloy 5083, Plate and Sheet;* SAE-AMS-QQ-A-250/6S; SAE International: Warrendale, PA, August 1998.

35. MIL-DTL-46027K. *Armor Plate, Aluminum Alloy, Weldable 5083, 5456, & 5059* **2007**.

36. *Aluminum Alloy Sheet and Plate 4.4CU - 1.5MG - 0.60MN (2024;-T3 Flat Sheet, -T351 Plate) Solution Heat Treated;* SAE-AMS4037; SAE International: Warrendale, PA, 2003.

37. Certification of Composition; AZ91C-T6-T6 per AMS-4437B, AMS B 80-01, Heat Number 635; Yankee Casting Co. Inc., Yankee Magcast Co.: Enfield, CT, August 2005.

38. ASTM G82-98. Standard Guide for Development and Use of a Galvanic Series for Predicting Galvanic Corrosion Performance. *Annu. Book ASTM Stand.* **2014.**

1 (PDF) DEFENSE TECHNICAL INFORMATION CTR DTIC OCA

2 (PDF) DIRECTOR US ARMY RESEARCH LAB RDRL CIO LL IMAL HRA MAIL & RECORDS MGMT

1 (PDF) GOVT PRINTG OFC A MALHOTRA

1 (PDF) RDRL ROE M S MATHAUDHU

1 (PDF) CORROSION POLICY AND OVERSIGHT OFC OF THE UNDER SECRETARY OF DEFNS FOR ACQUISITION TECHLGY AND LOGISTICS R HAYS

2 (PDF) UNIV OF VIRGINIA R KELLY J SCULLY

1 (PDF) MONASH UNIV N BIRBILIS

2 (PDF) OHIO STATE UNIV R BUCHHEIT G FRANKEL

1 (PDF) US NAVAL AIR WARFARE CMND V SANTIAGO C MATZDORF

1 (PDF) BAE SYSTEMS J DORSCH

1 (PDF) GENERAL DYNAMICS L KNISLEY

5 (PDF) DIR USARL RDRL WMM C J LABUKAS C MILLER B PLACZANKIS RDRL WMM D K CHO RDRL WMP E T JONES

INTENTIONALLY LEFT BLANK.